Microbiological Research 302 (2026) 128354

Contents lists available at ScienceDirect

Microbiological Research

journal homepage: www.elsevier.com/locate/micres

Identification of ShgH as a dual histidine/glutamine transporter component essential for *Streptococcus suis* virulence and biofilm modulation

Carla García [a,b], Luis Saralegui [a], Beatriz Morales [a], Paula Jurado [a], M. Teresa Bes [c,d], Clara Marín [b,e], Jesús Arenas [a,b,f,*]

[a] Unit of Microbiology and Immunology, Department of Animal Pathology, Faculty of Veterinary, University of Zaragoza (UNIZAR), Zaragoza, Spain
[b] Agrofood Research University Institute of Aragon (IA2), Zaragoza, Spain
[c] Department of Biochemistry and Molecular and Cellular Biology, Faculty of Science, UNIZAR, Zaragoza, Spain
[d] Institute for Biocomputation and Physics of Complex Systems (BIFI), Zaragoza, Spain
[e] Department of Animal Science, Agrofood Research and Technology Centre of Aragon (CITA), Zaragoza, Spain
[f] Aragón Health Research Institute (IIS) Aragón, Zaragoza, Spain

ARTICLE INFO

Keywords:
Streptococcus suis
ABC transport system
Histidine uptake system
Glutamine uptake system
Phagocytic activity
Biofilm formation
Virulence factor

ABSTRACT

Streptococcus suis is a zoonotic pathogen that affects pigs and humans. In this study, we characterised ShgH, a predicted substrate-binding component of an ABC transporter. Immunoassays confirmed that ShgH is expressed, secreted and surface-exposed in *S. suis,* in agreement with its proposed transporter function. Isothermal titration calorimetry demonstrated that ShgH binds glutamine and histidine, with a higher affinity for histidine. Deletion of the *shgH* gene significantly impaired uptake of both radiolabelled amino acids confirming its role as part of a transporter. Functional analysis revealed that *shgH* deletion results in a marked reduction in virulence in a murine infection model, while host colonization remained unaffected. ShgH contributes to infection by facilitating evasion of phagocytosis and resistance to oxidative stress through impaired nutrient acquisition and reduced capsule production. In addition, ShgH regulates biofilm formation and architecture. Notably, ShgH is highly conserved among pathogenic streptococci, suggesting a broader functional relevance. Altogether, our findings identify ShgH as a dual glutamine/histidine- binding protein essential for nutrient uptake and virulence in *S. suis*, and a promising target for future therapeutic interventions.

1. Introduction

Streptococcus suis is a Gram-positive bacterium commonly found as part of the commensal microbiota in the upper respiratory tract of swine. However, it can also act as a pathogen, causing bacteremia, endocarditis, arthritis, pneumonia, and meningitis (Haas and Grenier, 2018). Although the disease primarily affects weaning pigs; nursery pigs, fattening pigs and sows are also frequently affected. In Europe, approximately 80 % of pig production units are clinically affected by *S. suis* infections (Neila-Ibáñez et al., 2021). *S. suis* is also a zoonotic pathogen (Goyette-Desjardins et al., 2014) (Dong et al., 2021). Human infections often occur through raw or undercooked pork consumption or direct contact with infected pigs. It is one of the leading causes of bacterial meningitis in Vietnam, Thailand and China (Goyette-Desjardins et al., 2014; Tan et al., 2019), while incidence rates in Europe range from 0.1 to 4.9 cases per 100,000 individuals (Brizuela et al., 2024).

Treatment of *S. suis* infections relies primarily on antibiotics. However, due to its constant exposure to antimicrobials, both as a commensal and pathogen, clinical isolates often exhibit high levels of antimicrobial resistance, particularly to macrolides, lincosamides and tetracyclines (Uruén et al., 2022, 2023). Thus, alternative preventive strategies are urgently needed. Vaccination remains a promising approach, although current strategies are limited. Autogenous vaccines are widely used, but exhibit reduced efficacy due to the high genetic and antigenic diversity of *S. suis*. To date, more than 4200 Sequences Type (STs) have been identified by Multi Locus Sequence Type (MLST), which evidences the high genetic variability of this bacterium, complicating the development of broadly protective vaccines. Subunit vaccines targeting conserved antigens are under active investigation, but no effective commercial vaccine is currently available.

* Corresponding author at: Unit of Microbiology and Immunology, Department of Animal Pathology, Faculty of Veterinary, University of Zaragoza (UNIZAR), Zaragoza, Spain.
E-mail address: jaarenas@unizar.es (J. Arenas).

https://doi.org/10.1016/j.micres.2025.128354
Received 16 July 2025; Received in revised form 5 September 2025; Accepted 25 September 2025
Available online 26 September 2025

S. suis produces over 70 virulence factors, several of which have been extensively studied as potential vaccine targets (Segura, 2015). However, the expression of many of these factors is restricted to particular genetic lineages or geographic regions (Uruén et al., 2024). The best-characterized virulence factor is the polysaccharide capsule that plays a crucial role in evading phagocytosis. Up to 29 capsule types have been identified so far, which is the basis for serotyping. Nevertheless, only a few capsule types are associated with clinical disease (Votsch et al., 2018). The high variability of capsule types and limited long-term protection generated by capsule vaccines, have so far reduced its application as an effective vaccine component. As a result, the identification of novel and broadly protective antigens remains critical. In an effort to identify new virulence factors in *S. suis* with vaccine potential, our group previously conducted a transposon mutagenesis screen to identify conditionally essential genes for *S. suis* survival during experimental infection in pigs (Arenas et al., 2020). Among the genes identified was SSU0503, encoding a putative substrate-binding protein (SBP). This protein is part of an operon encoding a typical ABC transporter, which has not been characterized to date.

ABC transporters are membrane-spanning protein complexes that mediate the uptake of nutrients and export of molecules. A canonical ABC transporter is composed of two transmembrane domains (TMDs), two nucleotide-binding domains (NBDs) and one SBP, which may be membrane-anchored via a lipid or directly associated with the TMDs (Davidson et al., 2008). The transport begins when SBP binds its substrate, triggering a change in the conformation of TMD, which act as a permease, leading to the importing of the substrate through the membrane. Then, NBDs, which functions as an ATPase, lead to a return of the native conformation of the TMD (Davidson et al., 2008). Some ABC transporters have been shown to be essential for bacterial virulence, being key in host colonization (Akhtar and Turner, 2022), and few have even been proposed as vaccine candidates (Akhtar and Turner, 2022). In this work, we aimed to identify the biological function of SSU0503-encoding protein and determine its role in streptococcal disease. Our findings show that this protein functions as a histidine and glutamine binding protein that is conserved across multiple streptococcal species. Therefore, we propose to name it Streptococcal Histidine/Glutamine binding Protein (ShgH).

2. Material and methods

2.1. Bioinformatics

The signal peptide of ShgH encoded by SSU0503 in the reference strain of *S. suis* P1/7 was predicted using SignalP 5.0 (https://services.healthtech.dtu.dk/services/SignalP-5.0/). The surface exposed region of the protein was identified using TMHMM (https://services.healthtech.dtu.dk/services/TMHMM-2.0/), while the tertiary structure of was predicted using AlphaFold (https://alphafold.ebi.ac.uk/) and Phyre2 (https://www.sbg.bio.ic.ac.uk/phyre2/html/page.cgi?id=index). Sequence alignments were performed by the BLAST tool provided by NCBI (https://blast.ncbi.nlm.nih.gov/Blast.cgi) and the online MAFFT version 7 (https://mafft.cbrc.jp/alignment/server/index.html). For genetic conservation analyses, sequences from phylogenetically distant complete genomes were chosen. To avoid misinterpretations, only the assembled genomes at the chromosomal level were used. The number of analysed sequences was proportional to the total of sequences obtained for each specie. For comparative genomic analyses and conservation across species, Easyfig was used (https://mjsull.github.io/Easyfig/). Recombination points in *Streptococcus* DNA sequences were identified using RDP4 software suite (http://web.cbio.uct.ac.za/~darren/rdp.html). Break points were considered when at least three algorithm tests were positive. Molecular docking simulations between ShgH and its putative ligands were performed using SwissDock (http://old.swissdock.ch/docking), selecting the conformation with the lowest predicted binding energy. Docking images were adapted using PyMOL (https://www.pymol.org/).

2.2. Bacterial strains and growth conditions

The bacterial strains used in this study are listed in Table 1. *S. suis* strain P1/7 is considered a reference strain and its genome sequence is publicly available (Clifton-Hadley, 1984). It produces a serotype 2 capsule, and belongs to the ST1. *S. suis* strain P1/7Δ*gfp*$^{+}$ is a derivative of P1/7 that expresses a Green Fluorescent Protein (GFP) (manuscript in preparation) and P1/7Δ*cps2E-F* is an unencapsulated mutant derivative (Jurado et al., 2023). *S. suis* strains were grown in Todd-Hewitt Broth (THB, Condalab) supplemented with 5 g/L of peptone (Oxoid Ltd.). For solid media, THB was supplemented with 15 g/L of agar (Biokar Diagnostics) (THA). When required, antibiotics (Sigma-Aldrich) were added to the culture media, namely 100 μg/mL spectinomycin, 25 μg/mL chloramphenicol and 10 μg/mL tetracycline. For liquid cultures, *S. suis* was grown in THB at an initial optical density at 600 nm (OD_{600}) of 0.05 and incubated at 37ºC in a 5 % CO_2 atmosphere until reaching an OD_{600} of 0.5, which corresponds to the exponential growth phase. To evaluate *S. suis* growth under amino acid limited conditions, it was grown in a chemically defined medium (CDM) with varying concentrations of amino acids to which *S. suis* is auxotrophic (histidine, glutamine/glutamate, arginine, tryptophan and leucine), following the formulation previously described (Willenborg et al., 2015). All CDM components were obtained from Sigma-Aldrich. *S. suis* was growth overnight in THB, and then subcultured into fresh THB at an initial OD_{600} of 0.05 until reaching the logarithmic phase. Cells were harvested by centrifugation at 2500 g during 10 min, washed with Phosphate Buffer Saline (PBS, 7.7 mM Na_2HPO_4, 2.3 mM NaH_2PO_4, 145.5 mM NaCl, pH 7.35), and inoculated in CDM with varying amino acid concentration in 24-well plates at an initial OD_{600} of 0.05. Cultures were incubated at 37ºC during 24 h in a microplate reader (GENios Pro, Tecan) with OD_{600} measurements every 30 min. To asses bacterial growth under oxidative stress, *S. suis* was cultured in THB supplemented with 0.2 mM hydrogen peroxide (Panreac) at an initial OD_{600} of 0.02 in 96-well plates at 37ºC. Growth was monitored during 8 h using the microplate reader. The commercial *Escherichia coli* strain BL21 (DE3) (Invitrogen) was used for protein production. This bacterium was grown

Table 1
Strains used in this study.

Strain or Plasmid	Relevant characteristics	Source or reference
Strains		
S. suis		
P1/7	*S. suis* reference strain, serotype 2, ST1	(Clifton-Hadley, 1984)
P1/7Δ*cps2E-F*	P1/7 strain with *capE/G* genes replaced by *spec*^{R}	(Jurado et al., 2023)
P1/7Δ*shgH*	P1/7 strain with SSU0503 replaced by *spec*^{R}	This study
P1/7Δ*shgHc*	P1/7*shgH* strain with spec replaced by *shgH* gene and a *cat*^{R}	This study
P1/7Δ*gfp*$^{+}$	P1/7 expressing GFP with *tet*^{R}	Laboratory collection
P1/7Δ*gfp*$^{+}$Δ*shgH*	P1/7Δ*gfp*+ with SSU0503 replaced by *spec*^{R}	This study
E. coli		
BL21 (DE3)	Overexpression strain	Laboratory collection
BL21- pET16b-ssShgH	BL21 (DE3) strain with pET16b-ssShgH, *bla*^{R}	This study
Plasmids		
pET16b	Plasmid for expression of N-terminally His-tagged recombinant proteins in *E. coli*	Laboratory collection
pET16b-ssShgH	pET16b derivative encoding recombinant *S. suis* ShgH	This study

spec^{R}: spectinomycin-resistance cassette; *cat*^{R}: chloramphenicol-resistance cassette; *tet*^{R}: tetracycline-resistance cassette; *bla*^{R}: ampicillin resistant cassette.

at 37ºC in Luria Broth medium (LB, Sigma-Aldrich) or LB supplemented with 15 % of bacteriological agar (LBA), and, when required, with 100 μg/mL ampicillin. For liquid cultures, colonies from LBA plates were propagated in LB medium starting at an initial OD_{600} of 0.05, and incubated in a shaker incubator at 100 rpm until reaching an OD_{600} of 0.6–0.8. When required, 0.1 mM isopropyl β-D-1-thiogalactopyranoside (IPTG) was added to the culture medium to induce protein expression.

2.3. DNA constructs and preparation of mutants

All primers used in this study are listed in Table S1. To prepare knock-out mutants, DNA fragments upstream and downstream of the SSU0503 locus were amplified from chromosomal DNA of *S. suis* P1/7 using a High-Fidelity DNA Polymerase (Thermo Fisher Scientific). These fragments were fused to a spectinomycin-resistant cassette by overlap extension PCR using primers targeting the outermost regions following protocols described by us (García López et al., 2024). For genetic complementation, an additional fragment, containing the upstream region and the intact SSU0503, were amplified and fused to the downstream region of SSU0503 and a chloramphenicol-resistant cassette by PCR. Fluorescent mutants were generated by amplifying a DNA fragment encoding GFP protein from the fluorescent strain P1/7Δ*gfp*$^{+}$. PCR reactions were initiated with 5 min incubation at 98ºC for DNA denaturation, 30 cycles of 10 s at 98ºC, 30 s at 55ºC, an elongation at 72ºC (duration depending on the target amplicon, Table S1), and a final extension at 72ºC during 7 min. PCR products were separated in 1 % agarose gels and visualized using GelGreen nucleic acid strain (Biotium) in a bioimaging system. DNA fragments were purified using a silica column (QIAGEN) and used to transform *S. suis* P1/7, following previously described protocols (Zaccaria et al., 2014). Briefly, *S. suis* P1/7 was cultured overnight in THB at 37ºC, subcultured to an initial OD_{600} of 0.04, and mixed with 1.2 μg of transforming DNA and 250 μM of a ComX-Inducing Peptide (XIP) pheromone (GenScript) in a final volume of 100 μL. The mixture was incubated at 37ºC for 2 h, centrifuged (2500 g during 10 min), and plated on THA supplemented with antibiotics. Transformants were screened by PCR and confirmed by sequencing.

2.4. Purification of recombinant ShgH and antiserum production

The surface-exposed region of ShgH (amino acids 22–279) produced by *S. suis* strain P1/7 was produced as a recombinant protein using a heterologous expression system in *E. coli*. The DNA sequence encoding the mature protein was codon optimized for *E. coli* expression, cloned into the expression vector pET-16b (GenScript) with a 10-histidine tag added to its N-terminus to enable protein purification, and confirmed by sequencing. The resulting plasmid, called pET16b-ssShgH, was used to transform *E. coli* strain BL21 (DE3), and protein production was stimulated as described above. The recombinant ShgH was purified from bacterial lysates using Ni-NTA agarose affinity chromatography (QIAGEN GmbH), and dialyzed against PBS. Protein concentration was determined using the BCA Protein Assay kit (EMD Millipore Corp). Successful protein production and purification was assessed by SDS-PAGE, and the protein identity was verified by Western blotting using an anti-His tag antibody (as described below).

The purified recombinant ShgH was used to generate specific polyclonal sera in BALB/c mice (Janvier Labs) using a described protocol (Bosch et al., 2025). Briefly, 6 weeks old mice were immunized intraperitoneally with 50 μg of ShgH emulsified in a 1:1 ratio with 50 μg TiterMax Gold Adjuvant (Sigma-Aldrich) and administrated in two doses spaced two weeks apart. Two weeks after the final injection, mice were euthanized via CO_2 asphyxiation followed by cervical dislocation, and blood samples were collected. These animal experiments were approved by the Animal Welfare Committee of CITA (2019–03) and conducted in accordance with its guidelines and policies. Mice were housed in level II facilities at CITA, and fed and cleaned by certified personnel.

2.5. Sample preparation, SDS-PAGE and Western blotting

For all bacterial preparations, cells from logarithmic-phase cultures were used. For whole-cell lysate preparation, bacterial cells were harvested by centrifugation at 2500 g during 10 min. The resulting pellet was resuspended in PBS and adjusted to an OD_{600} of 10 for *S. suis* and 1 for *E. coli*. Cell envelope preparations and supernatants were obtained using previous described protocols (Arenas et al., 2015, 2016). Briefly, overnight cell cultures were centrifuged at 2500 g during 10 min. The pellet was resuspended in Tris-HCl (2 mM, pH 7.6), sonicated, centrifuged at 2500 g during 30 min and harvested by ultracentrifugation 20, 000 g during 3 h to obtain cell envelopes. Supernatants were precipitated with 10 % trichloroacetic acid (TCA) during 30 min on ice and centrifuged 10 min at full speed as previously described (Arenas et al., 2015). The pellet was washed with pure acetone, stored at −20ºC and resuspended in PBS. Samples were diluted in 4x sample buffer (0.25 M Base tris, 0.28 M SDS, 40 % glycerol, 6 mM bromophenol blue, 3 % ß-mercaptoethanol), denatured at 100ºC for 10 min, and subjected to SDS-PAGE using 12 % polyacrylamide gels. Electrophoresis was performed at 200 V during 45 min. Gels were either stained with Coomasie brilliant blue G250 (Thermo Fisher Scientific) or transferred to nitrocellulose membranes (Thermo Fisher Scientific) at 100 V for 60 min for Western blotting. Membranes were stained with Ponceau S (Sigma-Aldrich) to verify transfer efficiency, washed in PBS, and blocked for 1 h at room temperature with 3 % non-fat dry milk in PBS. Blots were incubated overnight at 4ºC with primary antibodies at working dilutions, including a commercial mouse monoclonal anti-GFP serum (Invitrogen), a commercial mouse monoclonal anti-His tag serum (Invitrogen), a mouse polyclonal anti-ShgH serum (this study), and a mouse polyclonal serum against the membrane protein GlnP (laboratory collection). After three washes in PBS, membranes were incubated for 1 h at room temperature with an HRP conjugated anti-mouse secondary antibody (Sigma-Aldrich). Signal detection was performed using Pierce ECL Western Blotting Substrate (NZYtech) and visualized in an iBright 1500 imaging system (Invitrogen).

2.6. Proteinase K accessibility assays

The surface accessibility of proteins was evaluated as previously described (Arenas et al., 2016), with minor modifications. *S. suis* strain P1/7Δ*gfp*$^{+}$ was cultured in THB to exponential phase and harvested by centrifugation at 2500 g during 10 min. Bacterial pellets were resuspended in PBS containing or not proteinase K (Invitrogen) at different concentrations, and incubated during 1 h at 37ºC. Bacterial cells were then centrifuged, washed with PBS, lysed, separated by SDS-PAGE and analysed by Western blotting.

2.7. Isothermal titration calorimetry assays

The interaction of ShgH with its potential ligands was assessed using an automated Auto-iTC200 high-sensitivity calorimeter (MicroCal, Malvern-Panalytical) following previous protocols (Bosch et al., 2025). Briefly, 200 μM of either L-histidine or L-glutamine were loaded into the injection syringe and titrated into a 40 μM solution of purified ShgH in a calorimetric cell. A standard titration consisted of a series of 19 sequential 2 μL injections at a rate of 0.5 μL/s, with a 150 s interval time spacing between injections. A reference power of 10 μcal/s and a stirring speed of 750 rpm were maintained throughout the experiment. Measurements were performed at 15ºC in PBS buffer. The binding isotherm was generated by integration of the thermogram after baseline correction. The association constant (K_a) and enthalpy change (ΔH) estimations were determined by fitting the data to a single-site binding model (1:1 stoichiometry) using non-linear least-squares regression data analysis with Origin 7.0 (OriginLab). The dissociation constant (K_d) was

calculated as the reciprocal of K_a. Gibbs free energy (ΔG) and entropy change (ΔS) were derived from K_d and ΔH, using standard thermodynamic equations. The background injection heat was accounted by including an adjustable constant parameter in the fitting function. The concentration of purified ShgH was determined spectrophotometrically using its theoretical extinction coefficient ($\varepsilon_{280\ nm} = 45{,}380\ M^{-1}cm^{-1}$).

2.8. Radiolabelled isotopes uptake assays

For radiolabelling experiments, bacterial strains from logarithmic phase cultures were harvested by centrifugation (2500 g during 10 min), washed twice with PBS, and subsequently cultured in CDM supplemented with 5 mg/L of histidine or glutamine and 1 μCi of ^{3}H-L-histidine or ^{3}H-L-glutamine adjusted at an OD_{600} of 0.1. Cultures were incubated during 1 h at 37ºC. Bacterial cells were then recovered and resuspended at an OD_{600} of 1 in histidine or glutamine deprived CDM to a final OD_{600} of 1, and mixed with Ultima Gold scintillation liquid (Sigma-Aldrich) at a 1:25 dilution. The incorporation rate of radiolabelled amino acid was quantified by measuring the ß-emission counts per minute (CPMB) using a Tri-Car 4810 TR Liquid Scintillation Analyzer (PerkinElmer) operated with QuantaSmart for Tri-Carb 5.2 software. Measurement parameters were optimized for ^{3}H with 1 min counting time and energy discrimination set between 2 keV (lower limit) and 18.6 keV (upper limit).

2.9. Macrophage cultures and phagocytosis assays

Phagocytic assays were performed using the murine macrophage cell line J774A.1, as previously described (Bosch et al., 2025). Shortly, cells were grown in DMEM medium supplemented with 1 % L-glutamine (GlutaMAX), 10 % foetal calf serum, and 1 % Penicillin/Streptomycin, all from Gibco. Macrophages were cultured at 37ºC in 5 % CO_2 in 25 cm^2 tissue-culture flasks (Nunc) until approximately 80 % confluence. Cells were detached by trypsinization and seeded in 24-well plates (Jet Biofil). After 24 h, cells were washed with Dullbecco's PBS (Invitrogen) and cultured for another 24 h in antibiotic-free DMEM supplemented with 1 % GlutaMAX, 1 % foetal calf serum and 1 ng/mL lipopolysaccharide from *E. coli* (Sigma-Aldrich) to activate the macrophages. *S. suis* from logarithmic-phase cultures were added to the activated macrophages at a multiplicity of infection (MOI) of 100 and incubated at 37ºC for 1 h. Before incubation, plates were centrifuged 800 g during 5 min to enhance macrophage-bacteria interaction. After incubation, non-adherent bacteria were removed by washing twice with commercial Dullbecco's PBS. To assess total macrophage-associated bacteria, cells were lysed with 1 % saponin in Dullbecco's PBS during 20 min, followed by mechanical disruption. Lysates were serially diluted and plated on THA plates for colony forming units (CFUs) counting. To assess intracellular bacteria, before saponin treatment, extracellular bacteria were killed by treatment with 120 μg/mL gentamicin during 1 h. To determinate intracellular survival, after 1 h gentamicin treatment, infected macrophages were washed and incubated for additional 2 h. The number of viable intracellular bacteria was determined by saponin treatment and CFU counting. The data are the average of three independent experiments with technical replicates. Results were expressed as a percentage of the initially inoculated bacteria.

2.10. Animal infections

Six-week-old CD1 mice (Janvier Labs) were housed in level II facilities at CITA and fed and cleaned by CITA personnel. After one-week adaptation, they were randomly assigned into 5-mice groups. Mice where shortly exposed to 1 % of acetic acid to irritate nostrils (Seitz et al., 2012). One hour later, the animals were intranasally inoculated with 1×10^7 CFUs of *S. suis* strains. Health, behaviour and weight were monitored daily to track clinical signs of streptococcal infection (depression, swollen eyes, rough hair coat, prostration and lethargy). Three days post infection, animals were euthanized using CO_2, followed by cervical dislocation. Nostrils and internal organs (lungs, heart, spleen, brain) were extracted, weighed, and homogenized in a Stomacher 80 (Seward). The number of viable bacteria was determined by serial dilution of samples in PBS and CFUs counting on THA plates. All animal experiments were approved by the Animal Welfare Committee of CITA (2023–01), and conducted in accordance with its guidelines and policies.

2.11. Biofilm formation

S. suis biofilm assays were performed as previously described (Jurado et al., 2023). Briefly, bacterial cells from logarithmic-phase cultures were resuspended in CDM with varying histidine and glutamine concentrations, adjusted at an OD_{600} of 1, and incubated in 24-well plates (Techno Plastic Products) at 37ºC during 24 h. Then, the supernatant was removed, and wells were washed with PBS. To quantify biofilm biomass, crystal violet staining was performed as described (Jurado et al., 2023). To examine biofilm by microscopy, biofilms were formed on glass, washed with PBS, and fixed in PBS containing 2 % formaldehyde for 1 h. Fixed samples were washed with PBS and visualized using a Leica TSC SP5 inverted microscope with an HCX PLAPO 40x/0.85 objective (Leica Microsystems). Image Z-stacks were acquired at 0.4 μm intervals and used to study biofilm architecture and structural parameters using COMSTAT software (Heydorn et al., 2000).

2.12. Determination of sialic acid

To demonstrate capsule loss in *S. suis,* sialic acid present on bacterial cell surface was quantified as described (Feng et al., 2012). Cell envelopes were extracted as described above, and adjusted to 2.5 mg/mL using a commercial BCA assay kit (Sigma-Aldrich). The sialic acid content was quantified using a commercial colorimetric kit (AssayGenie) following manufacturer's instructions.

2.13. Statistical analyses

For statistical comparisons, data were obtained from at least three independent experiments, each performed in duplicate. Statistical analyses were performed using an unpaired multiple *t*-test in GraphPad v6 software. Differences between groups were considered statistically significant when $p < 0.05$. P values were indicated with asterisks as $^*p < 0.05$, $^{**}p < 0.01$ or $^{***}p < 0.001$.

3. Results

3.1. Characterization and distribution of the shgH gene

Genomic analyses of the *S. suis* P1/7 genome indicates that SSU0503 locus is part of an operon, hereafter referred to as histidine/glutamine uptake operon (*hguo*). From 5´to 3´, *hguo* consists of three genes: SSU0501 (*shgP*), encoding a TMD; SSU0502 (*shgQ*), encoding a NBD; and SSU0503 (*shgH*), presumably encoding a SBP. Together, these genes likely form a classical ABC transporter. Upstream of the *hguo* operon, the SSU0500 (*glmS*) is located, which encodes a glutamine transaminase. A 152 bp intergenic region separates *glmS* from *hguo*. Within this region, we identified putative promoter elements, including a Pribnow box (TATACT) and a conserved −35 region (TTGAAA) (Figure S1). Multiple predicted transcription factor binding sites were also detected, including LrP, Fnr and RpoD (Figure S1). Interestingly, the region harbours consensus sequences recognized by amino acid responsive regulators, including GlnR (TGTTAAATTTATTAAA), involved in glutamine metabolism regulation (Kloosterman et al., 2006; Chen et al., 2010) (Figure S1). In addition, within the *glmS* gene, a consensus HisR sequence (CACTTTTGAGCAAAAAGCC) was detected, involved in histidine metabolism regulation (Ashniev et al., 2022) (Figure S1). The *glmS* gene is preceded by SSU0499 (*lepB*), encoding an endopeptidase,

SSU0498 (*axeA1*), encoding a GDSL lipase/esterase, and SSU0497 (*thi0*), encoding a FAD-binding oxidoreductase involved in amino acid transport. Downstream of *hguo*, SSU0506 encodes a metallo-hydrolase, and SSU0507, a bifunctional exonuclease/helicase. Between *shgH* and SSU0506, two pseudogenes encoding disrupted transposases belonging to the IS110 and ISL3 families were identified.

BLASTn analyses using the *hguo* as a query revealed hits in all 192 public *S. suis* genomes tested, with 100 % query coverages. Among these, 183 genomes exhibited sequence identities above 97.6 %, while the remaining nine ranged from 79.1 % to 95.4 % (Table 2). Homologous *hguo* operons were identified in other streptococcal species, including pathogens such as *S. pneumoniae* or *S. parasuis*, and non-pathogenic species like *S. mitis* and *S. cristatus*. In the selected genomes, the *hguo* operon showed a coverage of 91 % and sequence identities ranging from 66.5 % to 83 % (Table 2). Notably, the *S. suis hguo* shared high sequence identity (>80 %) with *S. parasuis* and *S. ruminantium*, but lower similarity (60 %-80 %) with *S. thermophilus, S. oriscaviae*, *S. pneumoniae*, and *S. oralis* (Table 2). The genetic context of the *hguo* operon in representative streptococcal species is illustrated in Fig. 1. The upstream region is relatively conserved among several species, including *S. suis, S. ruminantium, S. parasuis, S. oriscaviae, S. respiraculi, S. marmotae,* and *S. thermophilus*, particularly around the *glmS* gene. The region varies in length (2–4.55 kb) and sequence identity (71–84 %). In contrast, *S. oralis* and *S. pneumoniae,* display a divergent upstream region encoding genes such as ATP-synthase subunits (*atpB, F, H, A, G, D, C*), 6-phosphogluconolactonase (*pgl*), and an assembly-enhancing protease (*bepA*). The downstream region is highly variable across species. Some gene conservation was observed among *S. ruminantium* and *S. parasuis,* or *S. oriscaviae* and *S. respiraculi,* whereas *S. suis* shared no homology with other species in this region. Interestingly, *hguo*-like operons were identified in non-streptococcal species, such as *Clostridium butyricum*, *Clostridium perfringens* or *Clostridioides difficile*, although with low query coverage (<26 %).

The GC content of the *hguo* operon in *S. suis* was 39.1 %, closely matching the average GC content of the *S. suis* P1/7 genome (41.5 %). Prediction of recombination events within streptococcal sequences detected up to 12 recombination events in regions flanking the operon (indicated by thin arrows in Fig. 1). Three events were located downstream the *hguo*, involving *pepT* and *yidA* genes in *S. parasuis* H35 and *S. marmotae* HTS5, and *mtlD* and *fieF* in *S. respiraculi* HTS25 (Fig. 1). Six events were found upstream, generally spanning the region between *thi0* and *glmS* (Fig. 1). Within the *hguo* operon, three recombination events were identified in *S. suis, S. ruminantium* and *S. thermophilus.* In *S. suis*, the event involved the *glmS* gene and the intergenic region downstream *shgH*, with *S. thermophilus* 1 A or *S. parasuis* H35 as potential donors (Table S2). In *S. ruminantium* GUT183, the *thi0, axeA1, lepB* and *glmS* genes and the *hguo* operon appeared recombinant, with *S. parasuis* SUT380 and *S. suis* SC183 as likely sources (Table S2). In *S. thermophilus* 1 A recombination points flanked *hguo*, with *S. suis* P1/7 and *S. parasuis* H35 as potential donors (Table S2). No recombination events were detected in *S. oralis* FDAARGOS_885, *S. pneumoniae* 3641/15, and *S. oriscaviae* HKU75. Together, these data evidence that *hguo* is highly conserved in *Streptococcus* genus and suggest that horizontal gene transfer among certain streptococcal species has undergone.

Table 2
Distribution of *hguo* operon within 367 genome sequences of streptococcal species. *hguo* of *S. suis* P1/7 was used as query in BLAST searches. All tested genomes showed a query cover higher than 91 %.

Specie	Host	Pathogenic	Strains analysed	Identity percentage
S. suis	Swine, human	Yes	192	79.1–100
S. parasuis	Swine, human	Yes	4	82.1–82.4
S. ruminantium	Swine, human	Yes	2	82.9–83.1
S. respiraculi	Marmot	No	1	75.6
S. oriscaviae	Guinea pig	No	1	73.2
S. marmotae	Marmot	No	1	74
S. oralis	Human	No	6	67.6–71.1
S. pneumoniae	Human	Yes	30	71.2–71.6
S. mitis	Human	No	3	69.5–69.9
S. cristatus	Human	No	2	69.3–69.5
S. anginosus	Human	Yes	6	69.7–70.1
S. canis	Dog, cat, human	Yes	2	68.8
S. dysgalactiae	Swine, fish, cow, human, horse, seal	Yes	15	66.5–67.6
S. equi	Horse, swine, human, sheep	Yes	10	67.5–68.1
S. salivarius	Human	No	7	68.5–69.1
S. uberis	Cow, horse	Yes	2	69.2–69.4
S. pyogenes	Human	Yes	35	67.2–67.9
S. agalactiae	Cow, fish, human, camel, horse	Yes	20	67.5–68.7
S. iniae	Fish, dolphin, human	Yes	6	67.8–67.9
S. mutans	Human	No	8	68.6–68.8
S. thermophilus	Donkey, human	No	14	67.6–68.6

3.2. Three-dimensional model of S. suis ShgH

ShgH is a predicted lipoprotein of 278 amino acid residues in the *S. suis* reference strain P1/7. Its N-terminal extreme contains a signal peptide (residues 1–21) recognized by the Sec translocation machinery for crossing the membrane, followed by a conserved lipobox at position 22 (Fig. 2A, Figure S2), which becomes acylated to anchor the protein to the membrane. The mature lipoprotein contains an amino acid-binding domain spanning residues 38–268. Tertiary structure prediction using AlphaFold revealed that ShgH adopts a bipartite fold composed of two subdomains, S1 and S2, connected by a flexible linker (Fig. 2B). The N-terminal subdomain S1 contains six α-helices and seven β-sheets arranged in mixed orientations, while subdomain S2 consists on seven α-helices and five β-sheets forming a globular structure (Fig. 2B). Both subdomains contain small surface-accessible cavities, and a prominent central cavity located at their interface (Fig. 2C). This central cavity exposes multiple residues, suggesting a role in substrate binding. To investigate potential substrate specificity, structural homology searches were performed using Phyre2. ShgH exhibited high structural similarity to amino acid-binding proteins from other bacteria, including 74 % identity to a histidine-binding protein from *S. pneumoniae* (PDB: 4ohn), 65 % to a polar amino acid ABC uptake transporter from *S. thermophilus* (PDB: 3hv1), and 32 % to AncQR, a synthetic glutamine-binding protein (PDB: 4zv2). These results suggest that histidine and glutamine are likely substrates of ShgH.

To further investigate substrate binding of ShgH, molecular docking analyses were performed using ShgH in complex with histidine and glutamine (Fig. 2D). Polar interactions were assessed by identifying residues within 5 Å of each ligand in the central cavity of ShgH. Histidine was positioned to form polar interactions with four residues: Gly107, Ser109, Ser157 and Asp202. Additionally, hydrogen bonds were predicted between Ser109 and Arg114 with the oxygen atoms at positions 15 and 13 of histidine (Fig. 2E), respectively. These residues are also involved in ligand binding in the histidine-binding protein of *S. pneumonie* (PDB: 4ohn), confirming our predictions. In the glutamine-ShgH complex, six residues, including Asn106, Gly107, Ser109, Arg114, Ser157 and Asp202, were positioned for potential polar interactions. Notably, Arg114 and Ser157 were also predicted to form hydrogen bonds with the carbonyl oxygen of glutamine (Fig. 2E). All these residues involved in ligand binding were fully conserved in ShgH homologous from multiple Streptococcus species, including *S. oralis, S. pneumoniae, S. parasuis, S. oriscaviae, S. respiraculi, S. marmotae,* and *S. thermophilus* (Figure S2).

To further validate the role of specific residues in substrate binding, we compared predicted binding sites of ShgH with those of structurally characterized histidine- and glutamine-binding proteins from *E. coli.* In the crystal structure of the histidine-binding protein HisJ, nine residues

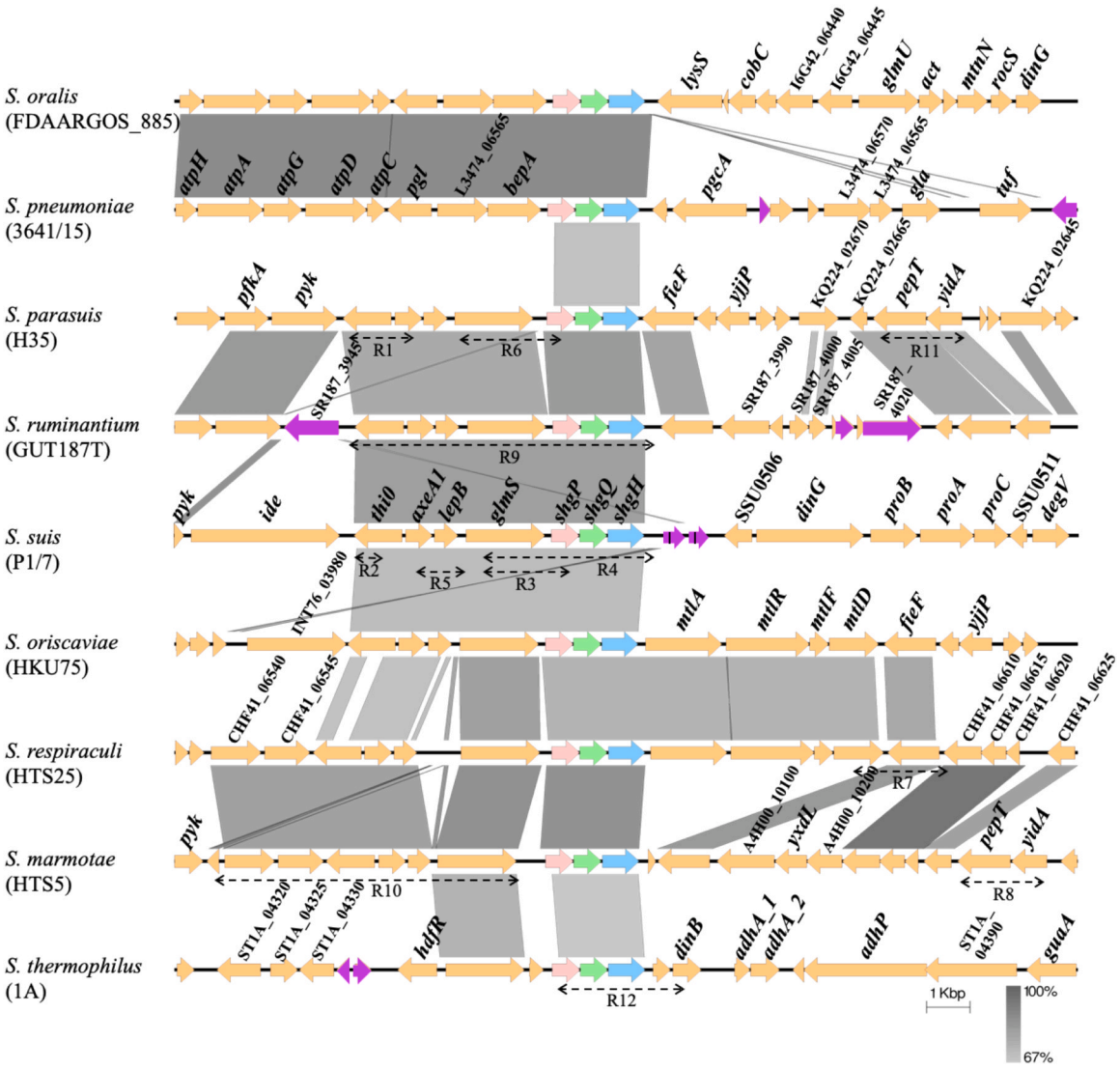

Fig. 1. Genomic context of *hguo* operon. Comparative analyses of the genomic context surrounding the *hguo* operon across various *Streptococcus* species. Gene names for *S. suis* P1/7 and homologous genes in other species are labelled. The *hguo* operon genes are coloured in pink (SSU0501), green (SSU0502), and blue (SSU0503). Transposases are indicated in violet. Gene conservation between species are shaded in grey. Thin arrows denote putative recombination events (R), further detailed in Table S2.

(Tyr14, Leu52, Ser69, Ser70, Ser72, Arg77, Leu117, Thr121, Asp161) were identified as critical for histidine interaction (Oh et al., 1994). The functional importance of several of these residues was confirmed through mutational analysis, demonstrating that Tyr14, Ser69 and Arg77 are involved in initial ligand binding, whereas Thr121 and Asp161 would contribute to ligand stabilization (Oh et al., 1994). Similarly, Yao et al. (1994) reported twelve histidine-binding residues (Tyr14, Leu52, Ser69, Ser70, Leu71, Ser72, Arg77, Leu117, Thr120, Thr121, Gln122, Asp161) in the active site of a histidine-binding protein from *E. coli* K12. D'Auria et al. (2008) identified nine residues (Asp7, Ala64, Gly65, Thr67, Arg72, Lys112, Gly116, His153, Asp154) relevant for glutamine recognition in GlnBP of *E. coli*. Thus, these three studies evidenced that two serine, an arginine and an aspartic acid appear critical for histidine binding, while an arginine, a threonine, a serine, and an aspartic acid are involved in glutamine binding. Notably, all these residues are conserved in *S. suis* ShgH (Figure S2). Together, these observations support the presence of a well-defined substrate-binding pocket in ShgH.

3.3. ShgH is located at the bacteria cell surface

To gain experimental insights into the production and location of ShgH in *S. suis* reference strain P1/7, we generated a recombinant version of the mature ShgH protein (residues 38–268), excluding the signal peptide. The recombinant protein was produced in *E. coli* and purified via Ni-NTA agarose affinity chromatography (Figure S3). The purified recombinant ShgH protein (28.9 kDa) was used to raise a specific polyclonal antiserum in mice. Western blot analysis confirmed that the antiserum specifically recognized recombinant ShgH (Fig. 3A). A band of similar size was detected in whole cell lysates of *S. suis* P1/7, in agreement with the expected molecular weight of native ShgH (31.1 kDa), and was absent in whole cell lysates from P1/7Δ*shgH* mutant (Fig. 3A). These results confirm that ShgH is indeed expressed by *S. suis* P1/7 under laboratory growth conditions.

To determinate the subcellular location of ShgH, whole-cell lysates, cell envelopes, and culture supernatants were prepared from P1/7 grown in THB. ShgH was detected in all three fractions, with the highest abundance in the culture supernatants (Fig. 3B). No substantial differences in molecular weight were detected across fractions. As a control,

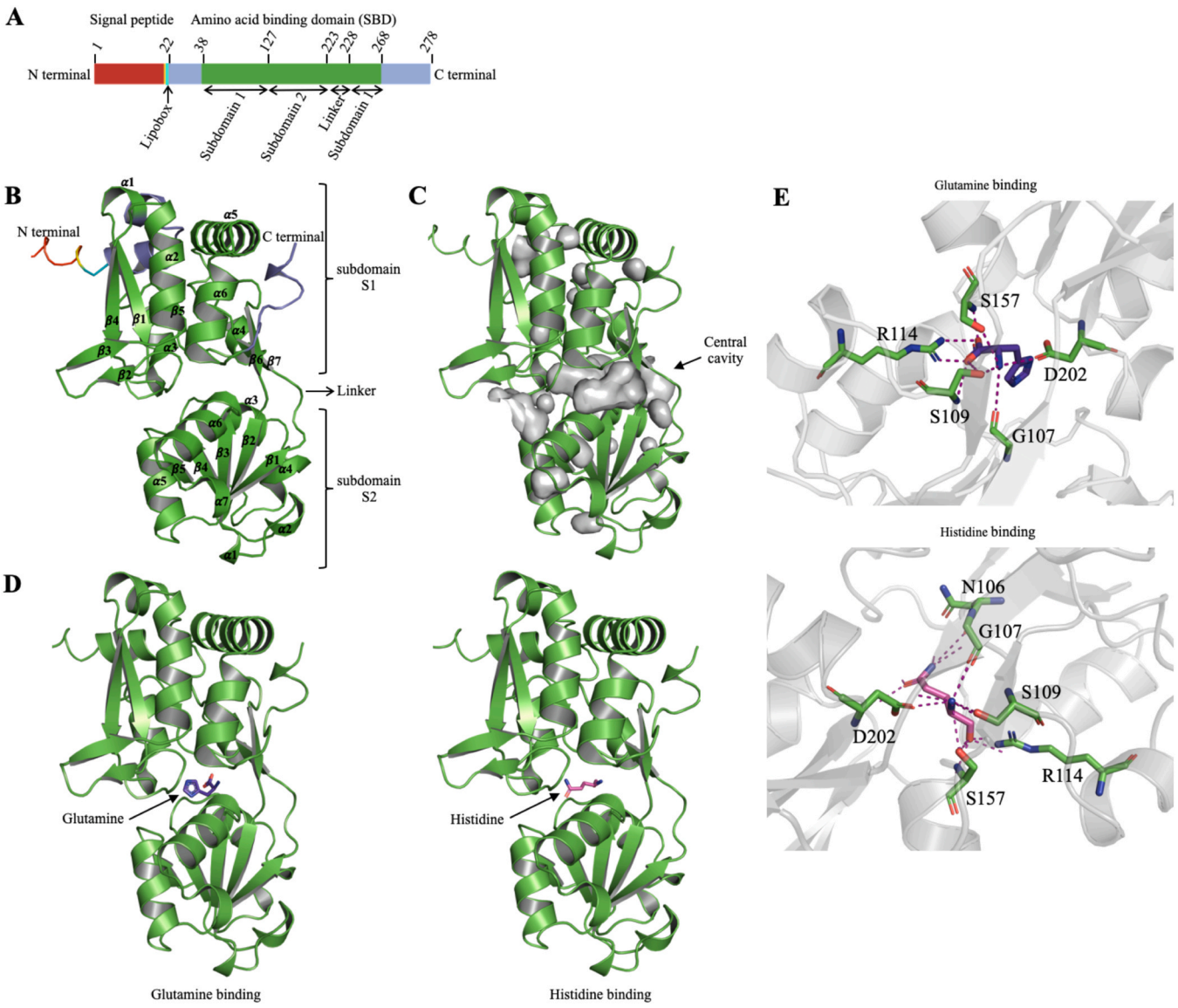

Fig. 2. ***In silico*** **prediction of ShgH structure.** (**A**) Schematic representation of domain distribution in the ShgH primary sequence. The N-terminal signal peptide (21 amino acids) is shown in red, and is followed by the conserved lipobox cysteine coloured in turquoise (amino acid 22). The predicted cleavage site as determined by SignalP2.0, located between amino acids 21 and 33 is shown in yellow. The amino acid-binding domain, comprising 230 amino acids, is shown in green. (**B**) Tertiary structure of mature ShgH generated using AlphaFold. Structural subdomains, designated as subdomain S1 and subdomain S2, are interconnected by a linker region. Secondary structure elements, including α-helices and β-sheets, are labelled and numbered. (**C**) Predicted surface cavities of ShgH are highlighted in grey. The major central cavity is indicated with an arrow. **(D)** Molecular docking of ShgH with histidine and glutamine. **(E)** Close-up view of 3D interactions of ShgH active site (green) with histidine (purple) or glutamine (magenta). Amino acid residues involved in ligand binding are labelled. Polar interactions and hydrogen bonds are shown in violet. Nitrogen atoms are depicted in dark blue, and oxygen atoms in red. Docking simulations were performed using SwissDock, and structural visualizations were generated and adapted in PyMOL.

the samples were probed with antiserum against the transmembrane protein GlnP, a membrane-associated permease (Arenas et al., 2020). GlnP was detected in whole-cell lysates and cell envelopes but not in culture supernatants (Fig. 3B). To investigate whether ShgH is surface-exposed, proteinase K accessibility assays were performed. Intact *S. suis* cells were treated with proteinase K, which degrades surface-exposed proteins but cannot penetrate intact bacterial membranes, preserving the integrity of cytosolic proteins. As a control, we used the *S. suis* strain P1/7Δ*gfp*$^{+}$, which produces a cytosolic recombinant GFP protein detectable by commercial anti-GFP antibodies. P1/7Δ*gfp*$^{+}$ cells were treated with 0.2 and 20 mg/L of proteinase K. ShgH was partially degraded at 0.2 mg/L and completely degraded at 20 mg/L, while GFP remained intact under both conditions (Fig. 3C). These results demonstrate that ShgH is indeed surface-exposed. Its presence in the extracellular medium suggests it may be released from the bacterial surface via an unknown mechanism.

3.4. *ShgH binds histidine and glutamine*

To experimentally probe the role of ShgH in histidine and glutamine transport, we took advantage of the fact that *S. suis* strain 10 is auxotrophic for both amino acids (Willenborg et al., 2015). We hypothesized that deletion of *shgH* would impair bacterial growth of *S. suis* strain P1/7 under histidine- and glutamine-limiting conditions. As a control, P1/7 and P1/7Δ*shgH* were grown in enriched THB medium, where exhibited similar growth (Fig. 4A). Growth was then compared in CDM. P1/7 grew well in CDM supplemented with 100 mg/L of histidine but failed to grow in the absence of histidine (Fig. 4B), confirming histidine auxotrophy.

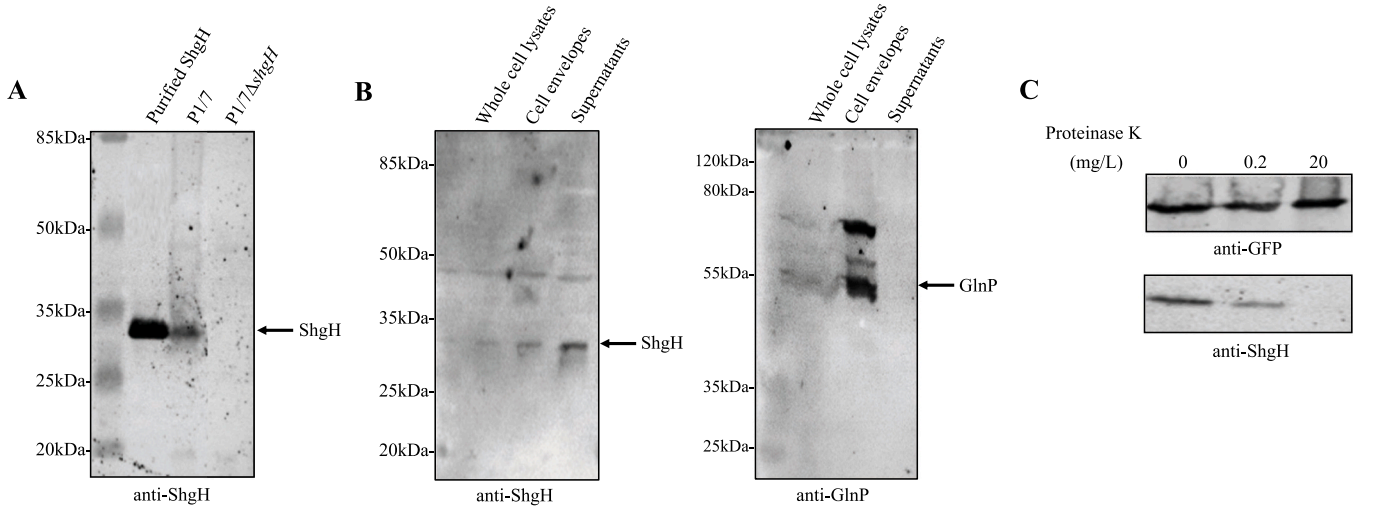

Fig. 3. Cellular localization and surface exposure of ShgH. (**A**) Western blot analysis of recombinant ShgH and whole-cell lysates of *S. suis* strain P1/7 and its derivative P1/7Δ*shgH* mutant against anti-ShgH serum. (**B**) Western blot analysis of whole-cell lysates, cell envelopes and supernatant preparations of *S. suis* strain P1/7 probed with anti-ShgH and anti-GlnP antibodies. GlnP serves as a membrane protein control. (**C**) Western blot analysis of whole-cell lysates from intact P1/7Δ*gfp*$^{+}$, which produces a recombinant cytoplasmic GFP protein serving as an internal control, after treatment with different concentrations of proteinase K. Blots were probed with anti-ShgH and anti-GFP antibodies to assess protein accessibility.

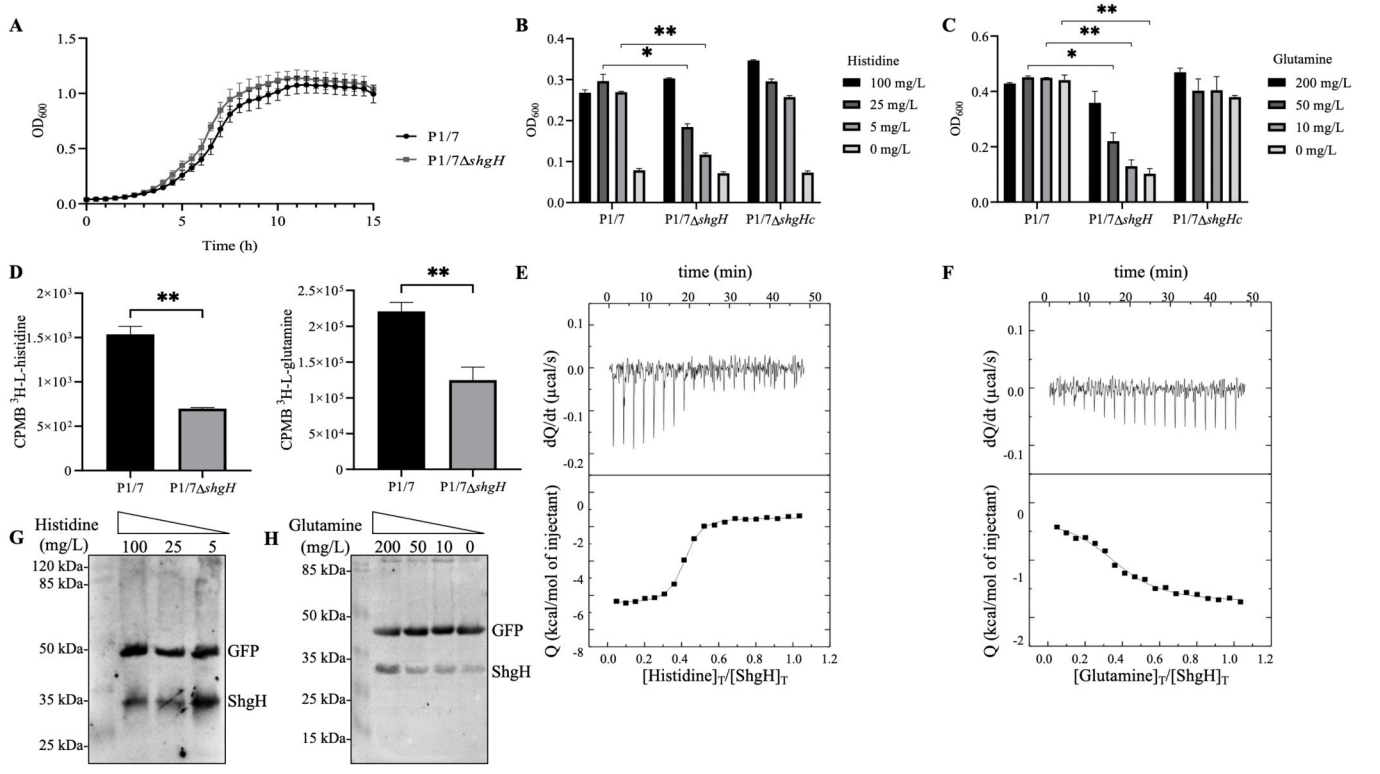

Fig. 4. ShgH is involved in glutamine and histidine uptake. (A) 15 h growth curve of *S. suis* P1/7 and the P1/7Δ*shgH* mutant in THB enriched medium. **(B-C)** Endpoint growth (measured after 12 h of incubation) of P1/7, P1/7Δ*shgH,* and the complemented strain P1/7Δ*shgHc* in chemical defined medium (CDM) with decreasing concentrations of (**B**) histidine or **(C)** glutamine. **(D)** ß-emission counts per minute (CPMB) from lysates of P1/7 and P1/7Δ*shgH* cultured in the presence of radiolabelled ^{3}H-L-histidine (left) and ^{3}H-L-glutamine (right). **(E-F)** Analysis of the interaction between purified ShgH and (**E**) histidine or **(F)** glutamine by isothermal titration calorimetry (ITC). Protein concentrations were determined by UV–visible spectrophotometry. ShgH (40 μM) was titrated with 200 μM of histidine and glutamine at 15ºC in PBS buffer. **(G-H)** Western blot analysis of whole-cell lysates of P1/7Δ*gfp*$^{+}$, which produces a cytoplasmic GFP protein as a control of loading, grown in CDM with decreasing concentrations of (**G**) histidine or **(H)** glutamine. Blots were probed with anti-ShgH serum. Data represent the mean ± standard deviation of three independent experiments with technical replicates. Statistical significance was assessed using an unpaired *t*-test. Asterisks show statistically significant differences between groups as *p < 0.05, **p < 0.01.

P1/7Δ*shgH* exhibited growth comparable to P1/7 in CDM at high histidine concentrations, but showed significantly reduced growth at lower histidine concentrations (Fig. 4B, and growth curve in Figure S4A). This phenotype was nicely restored when the *shgH* gene was reintroduced into the chromosome (P1/7Δ*shgHc* in Fig. 4B), confirming that the observed phenotype was not caused by adverse effects during transformation. Next, we monitored glutamine-dependent growth. Reduction of glutamine had no effect on P1/7 growth, probably due to the activity of glutamine synthetase, which enables glutamine synthesis from glutamate (Kloosterman et al., 2006). However, P1/7Δ*shgH* showed significantly reduced growth at lower concentrations of glutamine in a dose-dependent manner (Fig. 4C, and representative curve in Figure S4B). This phenotype was fully restored in the complemented strain (P1/7Δ*shgHc* in Fig. 4C). Notably, no growth differences were observed between P1/7 and P1/7Δ*shgH* under limiting conditions for other amino acids such as glutamate, leucine, arginine and tryptophan (Figure S4C-F), indicating the specificity of ShgH for histidine and glutamine transport.

To directly assess the role of ShgH in glutamine/histidine acquisition, we performed radiolabelled amino acid uptake assays. *S. suis* strains P1/7 and P1/7Δ*shgH* were cultured under histidine and glutamine restricted conditions and supplemented with ^{3}H-L-histidine or ^{3}H-L-glutamine. After incubation, cells were washed, lysed, and intracellular radioactivity was quantified. P1/7 accumulated significantly higher levels of ^{3}H-L-histidine (1536 ± 89 counts per minute of ß-radioactivity, CPMB) compared to the P1/7Δ*shgH* mutant (700 ± 12 CPMB) (Fig. 4D). Similarly, P1/7 showed markedly higher uptake of ^{3}H-L-glutamine (220,684 ± 12,520 CPMB) compared to P1/7Δ*shgH* (124,712 ± 18,032 CPMB) (Fig. 4D). These results confirm that ShgH is an essential component of the transporter system mediating the uptake of both amino acids.

To further characterize ShgH-ligand interactions, ITC assays were performed using purified recombinant ShgH (40 μM) titrated with either 200 μM L-histidine or L-glutamine at 15°C in PBS (Fig. 4E, F). ShgH bound L-histidine with high affinity showing a dissociation constant (K_d) of 0.17 μM and a binding enthalpy (ΔH) of −20.9 kJ/mol, indicating a dominant contribution of polar interactions such as hydrogen bonding and electrostatics. In contrast, binding to L-glutamine was weaker, with a K_d value of 3.5 μM, and a positive ΔH *of* 5.9 kJ/mol, suggesting a relevant role for hydrophobic interactions. These results confirm that

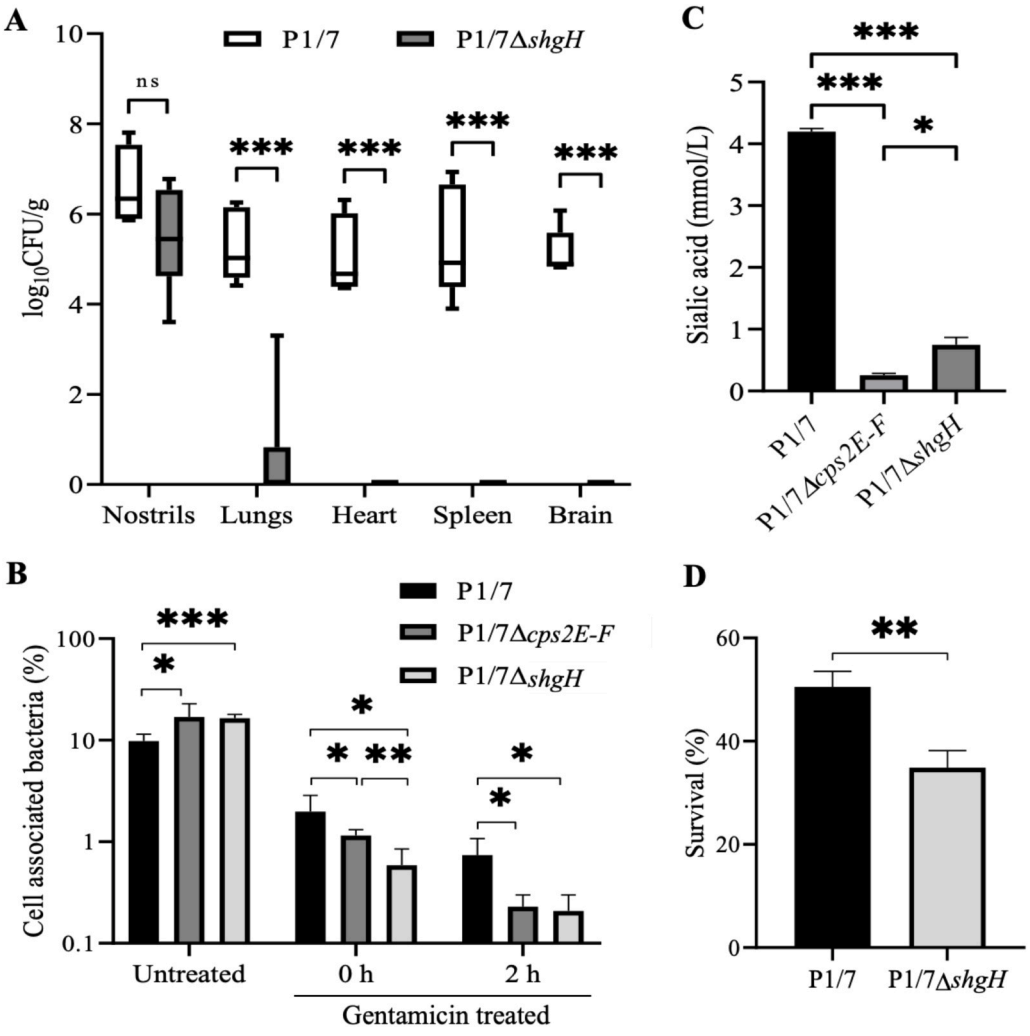

Fig. 5. Role of ShgH in *S. suis* virulence and phagocytosis. (A) Bacterial load of *S. suis* P1/7 and P1/7Δ*shgH* recovered from the nostrils and internal organs (lung, heart, spleen, brain) of CD1 mice following experimental infection. Colony-forming units (CFUs) were quantified, with each dot representing an individual mouse, and vertical lines indicating group averages. **(B)** Interaction of P1/7 and P1/7Δ*shgH* with J774 macrophage cells. The data show the percentages of cell-associated bacteria and intracellular bacteria at time 0 and after 2 h of gentamicin treatment, relative to the initial inoculum. **(C)** Sensitivity to oxidative stress measured by survival of P1/7 and P1/7Δ*shgH* in THB supplemented with 2 μM H_2O_2, expressed relative to survival in untreated control conditions. **(D)** Quantification of sialic acid in cell envelopes of P1/7, P1/7Δ*capE/G,* and P1/7Δ*shgH* determined using a colorimetric assay. Statistical analysis was performed using unpaired *t*-test and significant differences between groups are indicated with asterisks as follows: *p < 0.05, **p < 0.01, ***p < 0.001.

ShgH binds both histidine and glutamine.

Finally, we hypothesized that ShgH expression is regulated in response to histidine and glutamine availability, given the presence of predicted amino acid-responsive transcriptional regulators upstream of the *hguo* operon (Figure S1). To test this, ShgH production levels were analysed by Western blotting using whole cell lysates from P1/7Δ*gfp*$^{+}$ cultured in CDM with varying concentrations of histidine and glutamine. As shown in Fig. 4G, ShgH production increased about 2.5 folds at 5 mg/L of histidine compared to 100 mg/L, while GFP expression remained constant (internal control). In contrast, under glutamine-limiting conditions, ShgH expression decreased about four folds (Fig. 4H). Our data point out that ShgH expression is regulated by the concentrations of both amino acids.

3.5. ShgH is essential for S. suis virulence in a mouse infection model

Our previous transposon mutagenesis analyses identified *shgH* as conditionally essential gene for *S. suis* strain 10 virulence in pigs (Arenas et al., 2020). To further understand its role during infection, we performed intranasal challenge experiments using a murine model. Thus, CD1 mice were intranasally infected with equal doses of *S. suis* P1/7 or P1/7Δ*shgH*. Three days post-infection, bacterial loads were quantified in nostrils and internal organs. In the nasal cavity, about 10^7 and 10^6 CFU/g were recovered from P1/7- and P1/Δ*shgH*-infected mice, respectively. Notably, about 10^5 CFU/g of P1/7 disseminated to internal organs (lungs, heart, spleen, brain), in almost every infected mouse. In contrast, P1/7Δ*shgH* was hardly recovered from internal tissues (Fig. 5A). These results demonstrate that ShgH is essential for systemic dissemination of *S. suis*.

3.6. ShgH confers protection against phagocytosis and oxidative stress

We then wanted to gain insight into the mechanisms behind the role of ShgH in virulence. Phagocytosis is key in bacterial clearance by the host (Chabot-Roy et al., 2006), and, therefore, important in *S. suis* survival and infection capacity. Phagocytosis assays were performed using J774A.1 murine macrophages infected with *S. suis* P1/7, P1/7Δ*shgH* and a capsule-deficient control strain (P1/7Δ*cps2E-F*), as capsule type 2 protect *S. suis* against phagocytosis (Brazeau et al., 1996; Smith et al., 1999; Benga et al., 2008). After infection, cell-associated bacteria and intracellular bacteria were analysed by CFUs counting. About 1.47×10^6 CFUs/mL of P1/7 adhered to macrophages (about 10 % of the inoculum), which is significantly lower than 3.46×10^6 and 3.52×10^6 CFUs/mL of P1/7Δ*shgH* and P1/7Δ*cpsE-F,* respectively (Fig. 5B). At time 0, the number of intracellular P1/7 was 2×10^5 CFUs/mL (1.9 % of the inoculum), decreasing to 8.06×10^4 CFUs/mL (0.74 % of the inoculum) after 2 h. For P1/7Δ*shgH,* intracellular CFUs were 2.16×10^4 CFUs/mL (0.59 %) and dropped to 2.16×10^4 CFUs/mL (0.21 %) at 2 h. P1/7Δ*cps2E-F* showed 1.4×10^5 CFUs/mL and 5.64×10^4 CFUs/mL at time 0 and 2 h, respectively. Thus, deletion of *shgH* enhances bacterial adhesion to macrophages but impairs intracellular survival, similar to the capsule-deficient strain, suggesting a role for ShgH in resistance to phagocytic killing. Considering that P1/7Δ*shgH* showed a similar pattern as the unencapsulated derivative P1/7Δ*cps2E-F* (Fig. 5B), we hypothesized that *shgH* mutation could, somehow, alter capsule production. *S. suis* capsule 2 is composed of glucose, galactose, N-acetylglucosamine, rhamnose, and N-acetylneuraminic acid (*a.k.a.* sialic acid) (Van Calsteren et al., 2010). Quantification of sialic acid has been effectively used to demonstrate capsule loss in *S. suis* serotype 2 (Feng et al., 2012, Zhang et al., 2016). So, we quantified sialic acid in cell envelope fractions using a colorimetric assay. While P1/7 showed clear accumulation of sialic acid, both P1/7Δ*cpsE-F* and P1/7Δ*shgH* mutants showed only residual levels (Fig. 5C). These findings indicate substantial reduction in capsule production when absence of *shgH*. Given the importance of capsule in resisting phagocytic killing, we further hypothesized that reduced intracellular survival of P1/7Δ*shgH* could also result from increased sensitivity to oxidative stress, as previously observed in glutamine transporter mutants of *S. pneumoniae* (Hartel et al., 2011). To test this, we assessed bacterial survival in THB medium supplemented with 2 μM of H_2O_2. Indeed, P1/7Δ*shgH* showed a significant lower survival capacity (34.9 %) compared to the P1/7 strain (50.5 %) (Fig. 5D), supporting a role for ShgH in oxidative stress resistance.

3.7. ShgH modulates biofilm formation

Biofilm formation is important in bacterial colonization of the host, and in many pathogens is stimulated under nutrient-limited conditions (Ning et al., 2013; Raad et al., 2022). Furthermore, the absence of capsule stimulates biofilm formation in several species, including *S. suis* (Tanabe et al., 2010). Considering the relevant role of ShgH in nutrition acquisition and capsule production, we investigated whether it influences biofilm formation. First, biofilm formation was assessed in CDM supplemented with 100 mg/L of histidine or 200 mg/L of glutamine. Under these conditions, P1/7Δ*shgH* showed a modest but not statistically significant increase in biofilm formation compared to the wild-type strain (Fig. 6A). However, under nutrient-limited conditions (25 mg/L of histidine and 50 mg/L of glutamine) P1/7Δ*shgH* exhibited a significant enhanced biofilm formation relative to P1/7 (Fig. 6A). This phenotype was fully restored in the complemented mutant under histidine limitation and partially restored under glutamine limitation (Fig. 6A). To further characterize the effect of ShgH on biofilm architecture, confocal laser microscopy was performed at 24 h old biofilms formed by our GFP producing strains P1/7Δ*gfp*$^{+}$ and P1/7Δ*gfp*$^{+}$Δ*shgH*. The wildtype formed sparse, discrete clusters, while the *shgH* mutant developed dense, interconnected biofilms covering a significantly larger surface area (Fig. 6B). Quantitative analysis of biofilm architecture using COMSTAT evidenced that P1/7Δ*shgH* biofilms had significantly greater biomass, increased average thickness, and lower roughness coefficient compared to P1/7 (Fig. 6C). Together, these data show that ShgH modulates biofilm formation in *S. suis*.

4. Discussion

The SSU0503 gene was previously identified as essential for *S. suis* virulence in pigs (Arenas et al., 2020) but its specific biological function remained uncharacterized. In this study, we demonstrate that SSU0503 encodes ShgH, a SBP that is part of a dual ABC transporter system involved in the uptake of histidine and glutamine. This conclusion is supported by multiple experimental and *in silico* evidences. First, SSU0503 is located within an operon together with genes encoding a transposase and an ATPase (Fig. 1), consistent with the organization of a canonical ABC transporter. Second, *in silico* predictions, subcellular fractionation, and proteinase K accessibility assays revealed that ShgH is a lipoprotein exposed on the bacterial cell surface (Figs. 2A and 3), in agreement with its localization as a SBP involved in substrate recognition. Third, structural modelling predicted binding specificity for histidine and glutamine (Fig. 2B-D), which was experimentally validated using ITC (Fig. 4E, F). The functional role of ShgH in amino acid uptake was further supported by impaired growth of the *shgH* mutant under histidine- and glutamine-limited conditions (Fig. 4B, C), as well as reduced intracellular accumulation of ^{3}H-labelled substrates in uptake assays (Fig. 4D). Finally, ShgH production varied in response to external histidine and glutamine concentrations (Fig. 4G), which agrees with the presence of sequences for regulatory elements for amino acid-responsive transcription factor upstream of the operon (Figure S1).

Metagenomic studies of *S. suis* isolates from England, Vietnam and Spain have revealed extensive genomic diversity, with the core genome distributed across multiple Bayesian clusters and frequent signatures of recombination events (Weinert et al., 2015; Uruén et al., 2024). Many accessory genes encode virulence factors associated with specific lineages (Uruén et al., 2024), showing the evolutionary pressure to adapt to

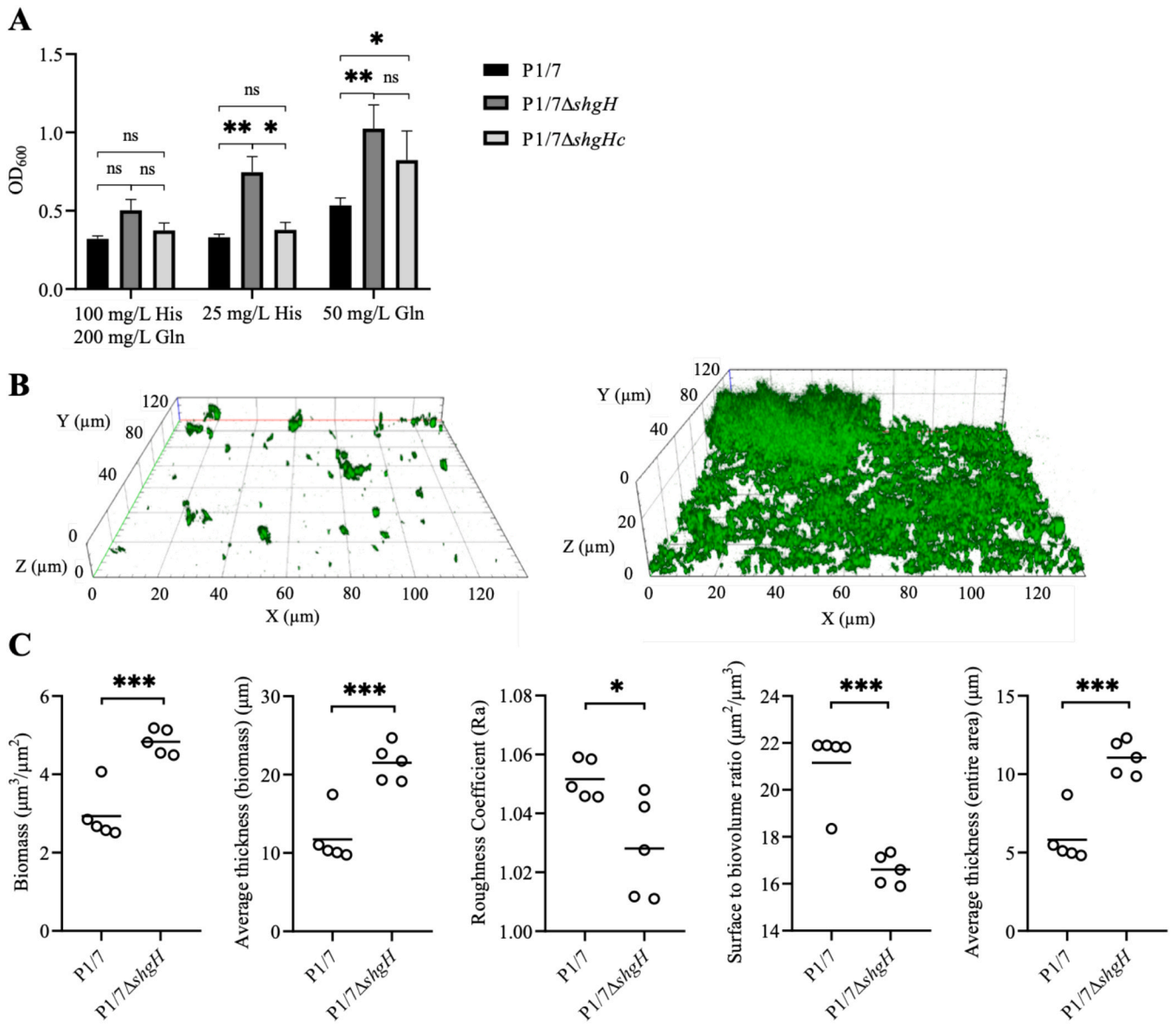

Fig. 6. Impact of ShgH on biofilm formation. (A) Biofilm biomass formed by P1/7, P1/7Δ*shgH* mutant, and the complement strain P1/7Δ*shgHc* after 24 h of growth in CDM or CDM with limiting concentrations of histidine or glutamine as indicated. **(B)** Spatial organization of 24h-biofilms formed by P1/7Δ*gfp*$^+$ and P1/7Δ*gfp*$^+$Δ*shgH* visualized through confocal laser scanning microscopy. **(C)** Quantitative parameters of the biofilm architecture of P1/7Δ*gfp*$^+$ and P1/7Δ*gfp*$^+$Δ*shgH*, including biomass, biomass thickness, roughness coefficient, surface to volume ratio and area thickness, determined using COMSTAT. Data represent individual measurements and mean values from five image stacks obtained from representative experiments. Statistical analysis was performed using unpaired t test. Asterisks indicate significant differences between both strains as *p < 0.05, **p < 0.01, *** p < 0.001. ns indicates non-significant differences (p > 0.05).

hosts and environments. In contrast, *hguo* is highly conserved across globally distributed *S. suis* genomes, showing minimal sequence variation (Table 2). This conservation supports its critical role in bacterial physiology and pathogenesis consistent with our TnSeq-based findings (Arenas et al., 2020). Homologous *hguo* operons were also found in multiple *Streptococcus* species, although the surrounding genomic context varies and includes transposase genes and recombination signatures, suggesting that the operon has undergone genetic mobilization from a common ancestor. In species such as *S. suis*, *S. parasuis*, *S. ruminantium*, *S. oriscaviae* or *S respiraculi, hguo* is co-located with conserved genes (*glmS, thi0, axeA1* and *lepB)* involved in cell wall biosynthesis (Kawada-Matsuo et al., 2012), biofilm formation (Aynapudi et al., 2017), signal peptide processing (Peng et al., 2001), and amino acid transport and metabolism (Molgaard et al., 2000; Kawada-Matsuo et al., 2016; Hammerstad and Hersleth, 2021). These streptococci share ecological niches as commensals or opportunistic pathogens of the upper respiratory tract. Thus, conservation of *hguo* and its genomic context likely reflects a shared role in nutrient acquisition and host colonization.

Our growth assays demonstrated that ShgH is essential for *S. suis* proliferation under histidine- and glutamine-limiting conditions, but dispensable when these amino acids are abundant. Radiolabelling uptake assays further revealed that ShgH contributes to 44 % of glutamine uptake (Fig. 4D), which is notably lower than glutamine transport systems in other species. For example, in *S. mutans*, the *glnQHMP* operon accounts for approximately 95 % of ^{3}H-glutamic uptake (Krastel et al., 2010). This lower efficiency may result from residual activity of the intact permease in the *hguo* operon, which was not inactivated in our mutant strain. The binding affinity of ShgH for L-glutamine (K_d=3.5 μM) is also lower than that reported for glutamine-binding proteins in other bacteria, such as *S. lactis* and *S. cremoris* (K_d=2.5 μM) (Poolman et al., 1987), or *E. coli* GlnBP (K_d=0.1 μM) (Chen et al., 2022). This relatively

lower affinity, combined with its endothermic binding profile, suggest that ShgH may function as part of a broader network of specific glutamine uptake transporters rather than as a primary transporter, as occurs in *S. pneumoniae,* where up to six glutamine transporters contribute distinctly to virulence and immune modulation (Hartel et al., 2011). Conversely, ShgH binds histidine in an exothermic manner with high affinity (K_d=0.17 μM), similar to well-characterized histidine-binding proteins such as *E. coli* HisJ (K_d=0.064–0.114 μM) (Chu et al., 2013; Paul et al., 2017), S typhimurium LAOBP (K_d=1.9 μM) and *Geobacillus stearothermophilus* ArtJ (K_d=0.42 μM) (Vahedi-Faridi et al., 2008; Pulido et al., 2015). Taken together, ShgH exhibits the characteristic profile of a dual-SBP with thermodynamically distinct binding modes, high-affinity exothermic binding for histidine, and lower-affinity endothermic binding for glutamine. This thermodynamic asymmetry is a hallmark of other dual transporters (Pulido et al., 2015; Paul et al., 2017), and likely reflects functional prioritization of histidine under limiting conditions, while glutamine uptake may represent a secondary or adaptive role under specific environmental conditions.

Our study shows that ShgH is present in extracellular fractions, and the molecular weight is nearly identical to that of the full-length protein. This suggest that ShgH is released from the bacterial surface rather than being proteolytically processed during secretion. This phenomenon is not novel, other *S. suis* lipoproteins, such as PrsA, have also been detected in extracellular fractions (Jiang et al., 2019). One putative mechanism involves variation at the conserved + 2 position of the lipobox motif, which influences membrane anchoring. In *Staphylococcus aureus*, substitutions at this position, particularly glycine or serine, have been associated with increased lipoprotein release into the exoproteome (Kumari et al., 2017). Notably, ShgH contains a glycine at this position (Figure S2), supporting this hypothesis. Alternatively, extracellular release could result from protease-mediated cleavage, a mechanism described for other bacterial lipoproteins such as NHBA (Serruto et al., 2010) or LbpB (Roussel-Jazede et al., 2010) in *Neisseria meningitidis*. Although the biological significance of ShgH release was not explored in this study, our ITC analysis, performed using a non-lipidated recombinant form of ShgH, demonstrated that its substrate-binding activity is retained. This suggest that extracellular ShgH may remain functional, sequestering amino acids from the environment, similarly to extracellular SBPs in Gram-negative bacteria (Davidson et al., 2008). Additionally, the release of ShgH could contribute to immune evasion, reducing antibody-binding to the membrane, as described for LbpB in *N. meningitidis* (Roussel-Jazede et al., 2010).

In this study, we elucidated the role of ShgH in *S. suis* infection. ShgH was essential for full virulence in a murine infection model (Fig. 5A). Glutamine is critical for protein and nucleotide synthesis, plays an important role in ammonium assimilation and serves as nitrogen donor in various biosynthetic reactions. Histidine is involved in protein and metabolite biosynthesis, and contributes to cellular pH maintenance and metal ion chelation. *S. suis* relies on environmental acquisition of both amino acids to grow (Willenborg et al., 2015). Previous studies have reported the concentrations of these amino acids in porcine serum and cerebrospinal fluid, resulting in 19.5 mg/L of histidine and 92 mg/L of glutamine in porcine serum, and 2 mg/L of histidine and 64.5 mg/L of glutamine in cerebrospinal fluid (Koczula et al., 2017). These concentrations are within the range where the *shgH* mutant displayed significant growth defects (Fig. 4B, C), supporting the hypothesis that ShgH contributes to virulence by facilitating nutrient uptake under host-relevant conditions. This is further supported by transcriptomic data showing *shgH* upregulation in porcine fluids (Koczula et al., 2017). In addition, ShgH impaired phagocytosis and intracellular survival in murine macrophages, likely due to high sensibility against oxidative stress conditions imposed by the macrophage in agreement with findings in *S. pneumoniae* glutamine transporter mutants (Hartel et al., 2011). Given the importance of phagocytosis in controlling *S. suis* infections (Chabot-Roy et al., 2006), this sensitivity likely contributes to attenuated virulence of the mutant. Furthermore, glutamine is required for β-D-N-acetylgalactosamine production in capsule biosynthesis (Kawada-Matsuo et al., 2016). Our sialic acid quantification assays confirmed that *shgH* deletion severely reduced capsule production (Fig. 5D), which is a known determinant of immune evasion in *S. suis* (Smith et al., 1999; Feng et al., 2012). This explains the similar phenotypes observed in the *shgH* mutant regarding macrophage adhesion, phagocytosis, intracellular survival and oxidative stress sensitivity (Fig. 5B), compared to uncapsulated mutant derivatives reported (Brazeau et al., 1996; Liu et al., 2020). Altogether, ShgH influences *S. suis* virulence through multiple mechanisms, including nutrient uptake, resistance to host immunity, and capsule biosynthesis.

The capsule has also been related to biofilm formation, an important factor in host colonization. Capsule deficient *S. suis* mutants form more robust biofilms than their wildtype (Ma et al., 2025), likely due to increased cell surface hydrophobicity, which promotes bacterial aggregation through adhesins and hydrophobic interactions (Tanabe et al., 2010). Nutrient limitation is another known trigger for enhanced biofilm formation in various organisms, including *Candida albicans* (Ning et al., 2013), *E. coli* (Culotti and Packman, 2014), and *Burkholderia contaminans* (Díaz et al., 2023). The enhanced biofilm formation capacity of the *shgH* mutant may be explained by the loss of capsule or reduced nutrient availability. Similar phenotypes have been reported for mutated glutamine transporters in other streptococci, such as SUB1152 in *S. uberis* (Crowley et al., 2011) or GlnP in *S. mutans* (Morikawa et al., 2020), with increased biofilm formation.

In conclusion, we have identified and characterized, for the first time, a novel SBP in *S. suis*, ShgH, and demonstrated its essential role in virulence and host colonization and the underlying molecular mechanisms. Considering its high level of conservation across multiple *Streptoccoccus* species, ShgH may represent a common virulence factor within the genus. These findings highlight ShgH as a promising target for the development of therapeutic or preventive strategies against streptococcal infections.

Author statement

CG designed and carried out experiments, analysed data, created tables and figures, and drafted the original manuscript. LS designed and generated mutant strains and conducted growth culture assays. BM and PJ carried out biofilm formation assays, and BM assisted with molecular docking and growth cultures. TB contributed to ITC experiments and data interpretation. CM performed mice immunizations and infection experiments. JA conceived and supervised the study, contributed to data analysis, reviewed and edited the manuscript, and acquired funding. All authors read and approved the final version of the manuscript.

CRediT authorship contribution statement

Beatriz Morales: Methodology. **Paula Jurado:** Methodology. **M. Teresa Bes:** Supervision, Software, Resources. **Clara Marín:** Supervision, Resources, Methodology. **Jesús Arenas:** Writing – review & editing, Visualization, Validation, Supervision, Resources, Project administration, Funding acquisition, Formal analysis, Data curation, Conceptualization. **Carla García:** Writing – original draft, Methodology, Investigation, Formal analysis, Data curation, Conceptualization. **Luis Saralegui:** Methodology, Investigation, Formal analysis, Data curation.

Funding

This work was supported by the Ciencia e Innovación/Agencia Española de Investigación MCIN/AEI/10.13039/501100011033 and, as appropriate, by ERDF A way of making Europe by the European Union or by the European Union NextGenerationEU/PRTR (Grant agreement PID2020–114617RB-100). The funders had no role in study design, data collection and analysis, decision to publish, or preparation of the manuscript.

Acknowledgements

We thank Juan Ignacio Aguiló (UNIZAR) for kindly provide murine macrophages lines used in this research. We acknowledge Cristina Uruén (UNIZAR) for her help in bioinformatic analysis and Santiago Morales (UNIZAR) for his support in radioactivity assays. Finally, we want to thank Adrián Velázquez-Campoy (BIFI) for his assistance in ITC analysis.

Appendix A. Supporting information

Supplementary data associated with this article can be found in the online version at doi:10.1016/j.micres.2025.128354.

Data availability

No data was used for the research described in the article.

References

Akhtar, A.A., Turner, D.P., 2022. The role of bacterial ATP-binding cassette (ABC) transporters in pathogenesis and virulence: therapeutic and vaccine potential. Micro Pathog. 171, 105734. https://doi.org/10.1016/j.micpath.2022.105734.

Arenas, J., Cano, S., Nijland, R., Van Dongen, V., Rutten, L., Van der Ende, A., Tommassen, J., 2015. The meningococcal autotransporter AutA is implicated in autoaggregation and biofilm formation. Environ. Microbiol. 17 (4), 1321–1337. https://doi.org/10.1111/1462-2920.12581.

Arenas, J., Paganelli, F.L., Rodríguez-Castaño, P., Cano-Crespo, S., Van der Ende, A., Van Putten, J.P., Tommassen, J., 2016. Expression of the gene for autotransporter AutB of *neisseria meningitidis* affects biofilm formation and epithelial transmigration. Front. Cell Infect. Microbiol. 6, 162. https://doi.org/10.3389/fcimb.2016.00162.

Arenas, J., Zomer, A., Harders-Westerveen, J., Bootsma, H.J., De Jonge, M.I., Stockhofe-Zurwieden, N., Smith, H.E., De Greeff, A., 2020. Identification of conditionally essential genes for *streptococcus suis* infection in pigs. Virulence 11 (1), 446–464. https://doi.org/10.1080/21505594.2020.1764173.

Ashniev, G.A., Sernova, N.V., Shevkoplias, A.E., Rodionov, I.D., Rodionova, I.A., Vitreschak, A.G., Gelfand, M.S., Rodionov, D.A., 2022. Evolution of transcriptional regulation of histidine metabolism in Gram-positive bacteria. BMC Genom. 23 (6), 558. https://doi.org/10.1186/s12864-022-08796-y.

Aynapudi, J., El-Rami, F., Ge, X., Stone, V., Zhu, B., Kitten, T., Xu, P., 2017. Involvement of signal peptidase I in *streptococcus sanguinis* biofilm formation. Microbiol. (Read.) 163 (9), 1306–1318. https://doi.org/10.1099/mic.0.000516.

Benga, L., Fulde, M., Neis, C., Goethe, R., Valentin-Weigand, P., 2008. Polysaccharide capsule and suilysin contribute to extracellular survival of *streptococcus suis* co-cultivated with primary porcine phagocytes. Vet. Microbiol 132 (1-2), 211–219. https://doi.org/10.1016/j.vetmic.2008.05.005.

Bosch, C., García, C., Saralegui, L., Van Beek, L., De Jonge, M.I., Marín, C., Arenas, J., 2025. Identification of the methionine transporter MetQ in *streptococcus suis* and its contribution to virulence and biofilm formation. Vet. Res 56 (1), 99. https://doi.org/10.1186/s13567-025-01522-y.

Brazeau, C., Gottschalk, M., Vincelette, S., Martineau-Doize, B., 1996. In vitro phagocytosis and survival of *streptococcus suis* capsular type 2 inside murine macrophages. Microbiol. (Read.) 142 (Pt 5), 1231–1237. https://doi.org/10.1099/13500872-142-5-1231.

Brizuela, J., Roodsant, T.J., Hasnoe, Q., Van der Putten, B.C.L., Kozakova, J., Slotved, H. C., Van der Linden, M., De Beer-Schuurman, I.G.A., Sadowy, E., Saez-Nieto, J.A., Chalker, V.J., Van der Ark, K.C.H., Schultsz, C., 2024. Molecular epidemiology of underreported emerging zoonotic pathogen *streptococcus suis* in Europe. Emerg. Infect. Dis. 30 (3), 413–422. https://doi.org/10.3201/eid3003.230348.

Chabot-Roy, G., Willson, P., Segura, M., Lacouture, S., Gottschalk, M., 2006. Phagocytosis and killing of *streptococcus suis* by porcine neutrophils. Micro Pathog. 41 (1), 21–32. https://doi.org/10.1016/j.micpath.2006.04.001.

Chen, P.M., Chen, Y.Y., Yu, S.L., Sher, S., Lai, C.H., Chia, J.S., 2010. Role of GlnR in acid-mediated repression of genes encoding proteins involved in glutamine and glutamate metabolism in *streptococcus mutans*. Appl. Environ. Microbiol 76 (8), 2478–2486. https://doi.org/10.1128/AEM.02622-09.

Chen, Q., Li, F., Zuo, X., Chen, J., Qin, P., Wang, C., Xu, J., Yang, D., Xing, B., Liu, Y., Jia, P., Li, L., Yang, C., Yu, D., 2022. Reversible domain closure modulates GlnBP ligand binding affinity. PLoS One 17 (4), e0263102. https://doi.org/10.1371/journal.pone.0263102.

Chu, B.C., De Wolf, T., Vogel, H.J., 2013. Role of the two structural domains from the periplasmic *escherichia coli* histidine-binding protein HisJ. J. Biol. Chem. 288 (44), 31409–31422. https://doi.org/10.1074/jbc.M113.490441.

Clifton-Hadley, F.A., 1984. Studies of *streptococcus suis* type 2 infection in pigs. Vet. Res Commun. 8 (3), 217–227. https://doi.org/10.1007/BF02214715.

Crowley, R.C., Leigh, J.A., Ward, P.N., Lappin-Scott, H.M., Bowler, L.D., 2011. Differential protein expression in *streptococcus uberis* under planktonic and biofilm growth conditions. Appl. Environ. Microbiol 77 (1), 382–384. https://doi.org/10.1128/AEM.01099-10.

Culotti, A., Packman, A.I., 2014. *pseudomonas aeruginosa* promotes *escherichia coli* biofilm formation in nutrient-limited medium. PLoS One 9 (9), e107186. https://doi.org/10.1371/journal.pone.0107186.

D'Auria, S., Staiano, M., Varriale, A., Gonnelli, M., Marabotti, A., Rossi, M., Strambini, G. B., 2008. The differences in the microenvironment of the two tryptophan residues of the glutamine-binding protein from *escherichia coli* shed light on the binding properties and the structural dynamics of the protein. Proteins 71 (2), 743–750. https://doi.org/10.1002/prot.21748.

Davidson, A.L., Dassa, E., Orelle, C., Chen, J., 2008. Structure, function, and evolution of bacterial ATP-binding cassette systems. Microbiol Mol. Biol. Rev. 72 (2), 317–364. https://doi.org/10.1128/MMBR.00031-07.

Díaz, A., Dixit, A.R., Khodadad, C.L., Hummerick, M.E., Justiano-Vélez, Y.A., Li, W., O'Rourke, A., 2023. Biofilm formation is correlated with low nutrient and simulated microgravity conditions in a *burkholderia* isolate from the ISS water processor assembly. Biofilm 5, 100110. https://doi.org/10.1016/j.bioflm.2023.100110.

Dong, X., Chao, Y., Zhou, Y., Zhou, R., Zhang, W., Fischetti, V.A., Wang, X., Feng, Y., Li, J., 2021. The global emergence of a novel *streptococcus suis* clade associated with human infections. EMBO Mol. Med 13 (7), e13810. https://doi.org/10.15252/emmm.202013810.

Feng, Y., Cao, M., Shi, J., Zhang, H., Hu, D., Zhu, J., Zhang, X., Geng, M., Zheng, F., Pan, X., Li, X., Hu, F., Tang, J., Wang, C., 2012. Attenuation of *streptococcus suis* virulence by the alteration of bacterial surface architecture. Sci. Rep. 2, 710. https://doi.org/10.1038/srep00710.

García López, C., Saralegui Remón, L., Uruén García, C., Bosch Díaz, C., Jurado Romero, P., Gottschalk, M., Arenas Busto, J., 2024. Techniques for genetic manipulation. Methods Mol. Biol. 2815, 37–49. https://doi.org/10.1007/978-1-0716-3898-9_4.

Goyette-Desjardins, G., Auger, J.P., Xu, J., Segura, M., Gottschalk, M., 2014. *streptococcus suis*, an important pig pathogen and emerging zoonotic agent - an update on the worldwide distribution based on serotyping and sequence typing. Emerg. Microbes Infect. 3 (6), e45. https://doi.org/10.1038/emi.2014.45.

Haas, B., Grenier, D., 2018. Understanding the virulence of *streptococcus suis*: a veterinary, medical, and economic challenge. Med Mal. Infect. 48 (3), 159–166. https://doi.org/10.1016/j.medmal.2017.10.001.

Hammerstad, M., Hersleth, H.P., 2021. Overview of structurally homologous flavoprotein oxidoreductases containing the low M(r) thioredoxin reductase-like fold - a functionally diverse group. Arch. Biochem Biophys. 702, 108826. https://doi.org/10.1016/j.abb.2021.108826.

Hartel, T., Klein, M., Koedel, U., Rohde, M., Petruschka, L., Hammerschmidt, S., 2011. Impact of glutamine transporters on pneumococcal fitness under infection-related conditions. Infect. Immun. 79 (1), 44–58. https://doi.org/10.1128/IAI.00855-10.

Heydorn, A., Nielsen, A.T., Hentzer, M., Sternberg, C., Givskov, M., Ersboll, B.K., Molin, S., 2000. Quantification of biofilm structures by the novel computer program COMSTAT. Microbiol. (Read.) 146 (Pt 10), 2395–2407. https://doi.org/10.1099/00221287-146-10-2395.

Jiang, X., Yang, Y., Zhou, J., Liu, H., Liao, X., Luo, J., Li, X., Fang, W., 2019. Peptidyl isomerase PrsA is surface-associated on *streptococcus suis* and offers cross-protection against serotype 9 strain. FEMS Microbiol Lett. 366 (2). https://doi.org/10.1093/femsle/fnz002.

Jurado, P., Uruén, C., Martínez, S., Lain, E., Sánchez, S., Rezusta, A., López, V., Arenas, J., 2023. Essential oils of *pinus sylvestris*, *citrus limon* and *origanum vulgare* exhibit high bactericidal and anti-biofilm activities against *neisseria gonorrhoeae* and *streptococcus suis*. Biomed. Pharm. 168, 115703. https://doi.org/10.1016/j.biopha.2023.115703.

Kawada-Matsuo, M., Mazda, Y., Oogai, Y., Kajiya, M., Kawai, T., Yamada, S., Miyawaki, S., Oho, T., Komatsuzawa, H., 2012. GlmS and NagB regulate amino sugar metabolism in opposing directions and affect *streptococcus mutans* virulence. PLoS One 7 (3), e33382. https://doi.org/10.1371/journal.pone.0033382.

Kawada-Matsuo, M., Oogai, Y., Komatsuzawa, H., 2016. Sugar allocation to metabolic pathways is tightly regulated and affects the virulence of *streptococcus mutans*. Genes (Basel) 8 (1). https://doi.org/10.3390/genes8010011.

Kloosterman, T.G., Hendriksen, W.T., Bijlsma, J.J., Bootsma, H.J., Van Hijum, S.A., Kok, J., Hermans, P.W., Kuipers, O.P., 2006. Regulation of glutamine and glutamate metabolism by GlnR and GlnA in *streptococcus pneumoniae*. J. Biol. Chem. 281 (35), 25097–25109. https://doi.org/10.1074/jbc.M601661200.

Koczula, A., Jarek, M., Visscher, C., Valentin-Weigand, P., Goethe, R., Willenborg, J., 2017. Transcriptomic analysis reveals selective metabolic adaptation of *streptococcus suis* to porcine blood and cerebrospinal fluid. Pathogens 6 (1). https://doi.org/10.3390/pathogens6010007.

Krastel, K., Senadheera, D.B., Mair, R., Downey, J.S., Goodman, S.D., Cvitkovitch, D.G., 2010. Characterization of a glutamate transporter operon, glnQHMP, in *streptococcus mutans* and its role in acid tolerance. J. Bacteriol. 192 (4), 984–993. https://doi.org/10.1128/JB.01169-09.

Kumari, N., Gotz, F., Nguyen, M.T., 2017. Aspartate tightens the anchoring of staphylococcal lipoproteins to the cytoplasmic membrane. Microbiologyopen 6 (6). https://doi.org/10.1002/mbo3.525.

Liu, L., Zhang, Q., Xu, Z., Chen, B., Zhang, A., Sun, X., Jin, M., 2020. Screening of Virulence-Related transcriptional regulators in *streptococcus suis*. Genes (Basel) 11 (9). https://doi.org/10.3390/genes11090972.

Ma, F., Wang, G., Ma, Z., Lin, H., Fan, H., 2025. A surface protein identified from *streptococcus suis* serotype 2 exhibits neutrophil-resistant ability via its polysaccharide capsule. Micro Pathog. 199, 107270. https://doi.org/10.1016/j.micpath.2024.107270.

Molgaard, A., Kauppinen, S., Larsen, S., 2000. Rhamnogalacturonan acetylesterase elucidates the structure and function of a new family of hydrolases. Structure 8 (4), 373–383. https://doi.org/10.1016/s0969-2126(00)00118-0.

Morikawa, Y., Morimoto, S., Yoshida, E., Naka, S., Inaba, H., Matsumoto-Nakano, M., 2020. Identification and functional analysis of glutamine transporter in *streptococcus mutans*. J. Oral. Microbiol 12 (1), 1797320. https://doi.org/10.1080/20002297.2020.1797320.

Neila-Ibáñez, C., Casal, J., Hennig-Pauka, I., Stockhofe-Zurwieden, N., Gottschalk, M., Migura-García, L., Pailler-García, L., Napp, S., 2021. Stochastic assessment of the economic impact of *streptococcus suis* - associated disease in German, Dutch and spanish swine farms. Front Vet. Sci. 8, 676002. https://doi.org/10.3389/fvets.2021.676002.

Ning, Y., Hu, X., Ling, J., Du, Y., Liu, J., Liu, H., Peng, Z., 2013. *candida albicans* survival and biofilm formation under starvation conditions. Int Endod. J. 46 (1), 62–70. https://doi.org/10.1111/j.1365-2591.2012.02094.x.

Oh, B.H., Kang, C.H., De Bondt, H., Kim, S.H., Nikaido, K., Joshi, A.K., Ames, G.F., 1994. The bacterial periplasmic histidine-binding protein. Structure/function analysis of the ligand-binding site and comparison with related proteins. J. Biol. Chem. 269 (6), 4135–4143. https://doi.org/10.1016/S0021-9258(17)41754-6.

Paul, S., Banerjee, S., Vogel, H.J., 2017. Ligand binding specificity of the *escherichia coli* periplasmic histidine binding protein, HisJ. Protein Sci. 26 (2), 268–279. https://doi.org/10.1002/pro.3079.

Peng, S.B., Wang, L., Moomaw, J., Peery, R.B., Sun, P.M., Johnson, R.B., Lu, J., Treadway, P., Skatrud, P.L., Wang, Q.M., 2001. Biochemical characterization of signal peptidase I from gram-positive *streptococcus pneumoniae*. J. Bacteriol. 183 (2), 621–627. https://doi.org/10.1128/JB.183.2.621-627.2001.

Poolman, B., Smid, E.J., Konings, W.N., 1987. Kinetic properties of a phosphate-bond-driven glutamate-glutamine transport system in *streptococcus lactis* and *streptococcus cremoris*. J. Bacteriol. 169 (6), 2755–2761. https://doi.org/10.1128/jb.169.6.2755-2761.1987.

Pulido, N.O., Silva, D.A., Téllez, L.A., Pérez-Hernández, G., García-Hernández, E., Sosa-Peinado, A., Fernández-Velasco, D.A., 2015. On the molecular basis of the high affinity binding of basic amino acids to LAOBP, a periplasmic binding protein from *salmonella typhimurium*. J. Mol. Recognit. 28 (2), 108–116. https://doi.org/10.1002/jmr.2434.

Raad, N., Tandon, D., Hapfelmeier, S., Polacek, N., 2022. The stationary phase-specific sRNA FimR2 is a multifunctional regulator of bacterial motility, biofilm formation and virulence. Nucleic Acids Res 50 (20), 11858–11875. https://doi.org/10.1093/nar/gkac1025.

Roussel-Jazede, V., Jongerius, I., Bos, M.P., Tommassen, J., Van Ulsen, P., 2010. NalP-mediated proteolytic release of lactoferrin-binding protein b from the meningococcal cell surface. Infect. Immun. 78 (7), 3083–3089. https://doi.org/10.1128/IAI.01193-09.

Segura, M., 2015. *streptococcus suis* vaccines: candidate antigens and progress. Expert Rev. Vaccin. 14 (12), 1587–1608. https://doi.org/10.1586/14760584.2015.1101349.

Seitz, M., Beineke, A., Seele, J., Fulde, M., Valentin-Weigand, P., Baums, C.G., 2012. A novel intranasal mouse model for mucosal colonization by *streptococcus suis* serotype 2. J. Med Microbiol 61 (Pt 9), 1311–1318. https://doi.org/10.1099/jmm.0.043885-0.

Serruto, D., Spadafina, T., Ciucchi, L., Lewis, L.A., Ram, S., Tontini, M., Santini, L., Biolchi, A., Seib, K.L., Giuliani, M.M., Donnelly, J.J., Berti, F., Savino, S., Scarselli, M., Costantino, P., Kroll, J.S., O'Dwyer, C., Qiu, J., Plaut, A.G., Moxon, R., Rappuoli, R., Pizza, M., Arico, B., 2010. *neisseria meningitidis* GNA2132, a heparin-binding protein that induces protective immunity in humans. Proc. Natl. Acad. Sci. USA 107 (8), 3770–3775. https://doi.org/10.1073/pnas.0915162107.

Smith, H.E., Damman, M., Van der Velde, J., Wagenaar, F., Wisselink, H.J., Stockhofe-Zurwieden, N., Smits, M.A., 1999. Identification and characterization of the cps locus of *streptococcus suis* serotype 2: the capsule protects against phagocytosis and is an important virulence factor. Infect. Immun. 67 (4), 1750–1756. https://doi.org/10.1128/IAI.67.4.1750-1756.1999.

Tan, C., Zhang, A., Chen, H., Zhou, R., 2019. Recent proceedings on prevalence and pathogenesis of *streptococcus suis*. Curr. Issues Mol. Biol. 32, 473–520. https://doi.org/10.21775/cimb.032.473.

Tanabe, S., Bonifait, L., Fittipaldi, N., Grignon, L., Gottschalk, M., Grenier, D., 2010. Pleiotropic effects of polysaccharide capsule loss on selected biological properties of *streptococcus suis*. Can. J. Vet. Res 74 (1), 65–70.

Uruén, C., García, C., Fraile, L., Tommassen, J., Arenas, J., 2022. How *streptococcus suis* escapes antibiotic treatments. Vet. Res 53 (1), 91. https://doi.org/10.1186/s13567-022-01111-3.

Uruén, C., Gimeno, J., Sanz, M., Fraile, L., Marín, C.M., Arenas, J., 2023. Invasive *streptococcus suis* isolated in Spain contain a highly promiscuous and dynamic resistome. Front Cell Infect. Microbiol 13, 1329632. https://doi.org/10.3389/fcimb.2023.1329632.

Uruén, C., Fernández, A., Arnal, J.L., Del Pozo, M., Amoribieta, M.C., De Blas, I., Jurado, P., Calvo, J.H., Gottschalk, M., González-Vázquez, L.D., Arenas, M., Marín, C.M., Arenas, J., 2024. Genomic and phenotypic analysis of invasive *streptococcus suis* isolated in Spain reveals genetic diversification and associated virulence traits. Vet. Res 55 (1), 11. https://doi.org/10.1186/s13567-024-01267-0.

Vahedi-Faridi, A., Eckey, V., Scheffel, F., Alings, C., Landmesser, H., Schneider, E., Saenger, W., 2008. Crystal structures and mutational analysis of the arginine-, lysine-, histidine-binding protein ArtJ from *geobacillus stearothermophilus*. Implications for interactions of ArtJ with its cognate ATP-binding cassette transporter, Art(MP)2. J. Mol. Biol. 375 (2), 448–459. https://doi.org/10.1016/j.jmb.2007.10.049.

Van Calsteren, M.R., Gagnon, F., Lacouture, S., Fittipaldi, N., Gottschalk, M., 2010. Structure determination of streptococcus suis serotype 2 capsular polysaccharide. Biochem Cell Biol. 88 (3), 513–525. https://doi.org/10.1139/o09-170.

Votsch, D., Willenborg, M., Weldearegay, Y.B., Valentin-Weigand, P., 2018. *streptococcus suis* - the "two faces" of a pathobiont in the porcine respiratory tract. Front Microbiol 9, 480. https://doi.org/10.3389/fmicb.2018.00480.

Weinert, L.A., Chaudhuri, R.R., Wang, J., Peters, S.E., Corander, J., Jombart, T., Baig, A., Howell, K.J., Vehkala, M., Valimaki, N., Harris, D., Chieu, T.T., Van Vinh Chau, N., Campbell, J., Schultsz, C., Parkhill, J., Bentley, S.D., Langford, P.R., Rycroft, A.N., Wren, B.W., Farrar, J., Baker, S., Hoa, N.T., Holden, M.T., Tucker, A.W., Maskell, D. J., Consortium, B.R.T., 2015. Genomic signatures of human and animal disease in the zoonotic pathogen *streptococcus suis*. Nat. Commun. 6, 6740. https://doi.org/10.1038/ncomms7740.

Willenborg, J., Huber, C., Koczula, A., Lange, B., Eisenreich, W., Valentin-Weigand, P., Goethe, R., 2015. Characterization of the pivotal carbon metabolism of *streptococcus suis* serotype 2 under ex vivo and chemically defined in vitro conditions by isotopologue profiling. J. Biol. Chem. 290 (9), 5840–5854. https://doi.org/10.1074/jbc.M114.619163.

Yao, N., Trakhanov, S., Quiocho, F.A., 1994. Refined 1.89-A structure of the histidine-binding protein complexed with histidine and its relationship with many other active transport/chemosensory proteins. Biochemistry 33 (16), 4769–4779. https://doi.org/10.1021/bi00182a004.

Zaccaria, E., Van Baarlen, P., De Greeff, A., Morrison, D.A., Smith, H., Wells, J.M., 2014. Control of competence for DNA transformation in *streptococcus suis* by genetically transferable pherotypes. PLoS One 9 (6), e99394. https://doi.org/10.1371/journal.pone.0099394.

Zhang, Y., Ding, D., Liu, M., Yang, X., Zong, B., Wang, X., Chen, H., Bei, W., Tan, C., 2016. Effect of the glycosyltransferases on the capsular polysaccharide synthesis of *streptococcus suis* serotype 2. Microbiol Res 185, 45–54. https://doi.org/10.1016/j.micres.2016.02.002.